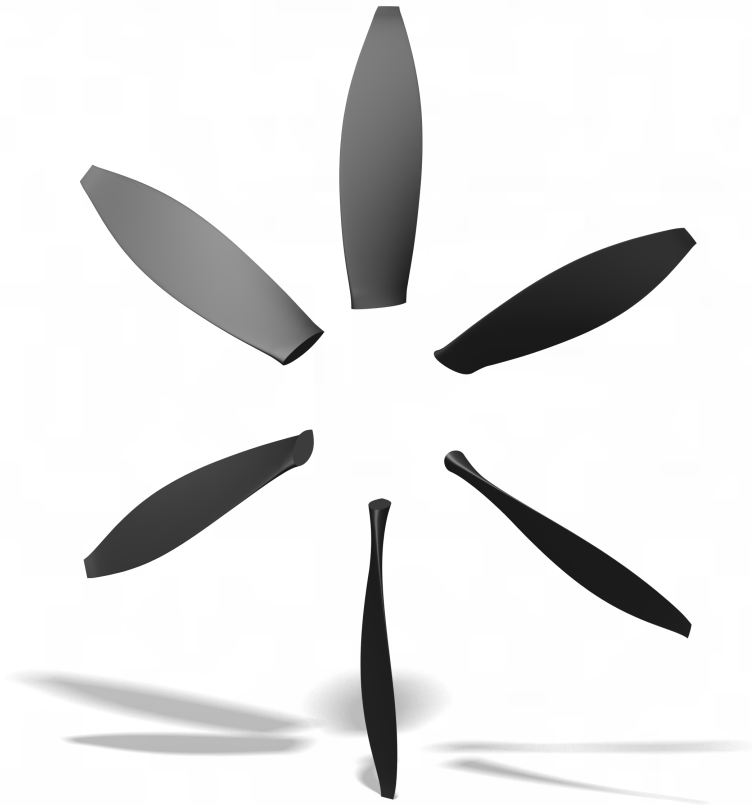# Low-Noise Propeller Design for Future Electric Aircraft

A numerical study on propeller efficiency and noise emissions

Bachelor's thesis in Mechanical Engineering

Mohamed Hadi Haidari
Felix Hövik
Caspian Lago
Fredrik Nyström Lindé
Jacob Sjöberg

Low-Noise Propeller Design for Future Electric Aircraft

A numerical study on propeller efficiency and noise emissions

Mohamed Hadi Haidari

Felix Hövik

Caspian Lago

Fredrik Nyström Lindé

Jacob Sjöberg

CHALMERS
UNIVERSITY OF TECHNOLOGY

Department of Mechanics and Maritime Sciences
Division of Fluid Dynamics
CHALMERS UNIVERSITY OF TECHNOLOGY
Gothenburg, Sweden 2020

Low-Noise Propeller Design for Future Electric Aircraft
A numerical study on propeller efficiency and noise emissions
Mohamed Hadi Haidari, Felix Hövik, Caspian Lago, Fredrik Nyström Lindé, Jacob Sjöberg

Cover: Model of baseline propeller created in CATIA V5.

Low-Noise Propeller Design for Future Electric Aircraft
A numerical study on propeller efficiency and noise emissions
Mohamed Hadi Haidari, Felix Hövik, Caspian Lago, Fredrik Nyström Lindé, Jacob Sjöberg
Department of Mechanics and Maritime Sciences
Chalmers University of Technology

Abstract

Right now electric aircraft are being developed as an alternative to make the aviation industry more sustainable. The electric airplanes available today are using propellers connected to an electric engine as the main propulsion system, and thus the propeller is a critical part of the airplane. This numerical study aims to give a better understanding on how to create propellers optimized for electric aircraft with minimum energy loss and noise emissions.

An existing propeller design methodology, implemented in the MATLAB environment as *OptoProp*, is applied to design a propeller with optimum efficiency. A documented case is then used to verify the applied program. Afterwards, the program is utilised to conduct a parameter study where one or multiple parameters at a given thrust are alternated, and also studying the usage of multiple propellers. Then, the calculated data is used as input for the noise simulations. The results from the parameter study indicates that increasing an individual parameter leads to an improved aerodynamic performance. When testing multiple parameters the positive results from increasing each parameter value continues to a certain point after which the propeller performance decreases. When studying multiple propellers it was found that optimal efficiency is achieved with a four propeller setup.

During this project tools used to simulate propeller noise have been developed in a MATLAB environment. The programs are verified by comparing the results to previously documented cases and then used to study sound emissions of single propellers with varying parameters. The results from this study show the impact each parameter has on the noise levels and their correlation with the tip Mach number should be considered. Lastly, sound emissions of multiple propellers and different propeller distributions are studied. This study indicates that the impact on noise far away from the propellers is almost insignificant whereas the noise close to the propellers generally decreases with an increasing number of propellers.

Since the conclusions from the two studies differ, compromises had to be made in order to propose guidelines, taking the results from both studies into account. The guidelines contain recommendations for an optimal propeller design, balancing the choice between high efficiency and reduced noise pollution.

Keywords: low-noise propeller, electric aircraft, propeller design, acoustic studies.

Acknowledgements

This report is the result of a bachelor's thesis performed by students from the programs Mechanical Engineering and Engineering Physics. The project was done under the division of Fluid Dynamics at Chalmers University of Technology.

The group working on this project would like to thank our supervisor Dr. Zhongjie Huang and to express our gratitude to Alexandre Capitao Patrao, the creator of the *OptoProp* program.

<div align="right">

Mohamed, Felix, Caspian, Fredrik, Jacob
Gothenburg, May 2020

</div>

Contents

List of Figures

List of Tables

Nomenclature and Abbreviations

a	Axial interference factor
a'	Rotational interference factor
B	Number of propeller blades
c	chord
c_0	Sound speed
C_D	Drag coefficient
C_L	Lift coefficient
C_l	Blade section lift coefficient
C_T	Thrust coefficient
C_{Do}	Zero-lift drag coefficient
D	Diameter of the propeller
D'	Drag force per unit radius
D_c	Total drag
e	Oswald efficiency factor
F	Prandtl momentum loss factor
G	Circulation function
H	Flight altitude of propeller at cruise
J_{mB}	Bessel function of first kind with index mB
L'	Lift force per unit radius
M	Mach number
m	Harmonic number
M_{tip}	Helical tip Mach number
n	Rotational speed
P	Power
p'_Q	Pressure associated with torque
p'_T	Pressure associated with thrust
p'_{rms}	Root-mean-square pressure
Q	Torque
S	Reference area of wing
T	Thrust
t	Thickness
T_c	Total thrust
U_{tip}	Tip speed
V_∞	Free stream velocity of the fluid
W	Local total velocity
w_n	Normal velocity (to vortex sheet)

w_t	Tangential velocity
W_{to}	Maximum take-off weight
W_{to}	Maximum takeoff weight
x	Nondimensional distance
y_1, y_2	Length of the chord on respective side of the point of maximum thickness
y_c	Vertical distance between chordline and camberline

β	Blade angle
ϵ	Drag-to-lift ratio
η	Efficiency
Γ	Circulation
λ	Aspect ratio of wing
Ω	Angular velocity
ω	Rotational velocity
ϕ	Flow angle
ϕ_t	Flow angle at tip
ρ	Density
ξ	Nondimensional radius
ξ_0	Nondimensional hub radius
ζ	Displacement velocity ratio

CFD	Computational Fluid Dynamics
FW-H	Ffowcs Williams and Hawkins equation
HTR	Hub-Tip Ratio
RPM	Revolutions Per Minute
RPS	Revolutions Per Seconds
SPL	Sound Pressure Level

1

Introduction

Pressure from the public and legislators constructing stricter environmental restrictions has pushed the aviation industry to commit to energy optimization and electrification of conventional aircraft. This has resulted in an opening for the innovation of new technologies within the electric vehicle industry. The advancement of electrified aircraft using the open-rotor engine has lead to this setup being vastly more available and used. There is now a great interest in improving the efficiency and minimising the noise radiation from these airplanes.

1.1   Background

Environmental topics are becoming more and more popular around the world and the aviation industry is not exempt from this discussion. Aviation has a big impact on the environment and is today responsible for about 2% of global CO_2 emissions [1]. Flights under 1500 kilometers, also known as short-haul flights, stand for 20% of the CO_2 emissions by aviation [2]. The CO_2 emissions are expected to increase in the coming years as the number of passengers per year is estimated to double by 2037 [3]. The challenge that lies ahead is to meet harder requirements on fuel consumption, pollution, gas emission and noise radiation from aviation legislators.

Inspired by the electrification in the automotive industry, the aviation industry is now looking into the electrification of aircraft, due to the low operating costs and zero emissions. Electric aircraft are believed to be the solution for more sustainable short-haul flights. Electrification also makes new innovative concepts of aircraft feasible.

1.2   Problem

The aviation industry is making a transition into electrification of aircraft which creates an abundance of complications. The challenge with electric aircraft is that flight range have to be significantly increased before they can be used commercially. The limited range is due to batteries not being able to store enough specific energy to keep the plane in the air for long periods of time, batteries can only store about 250 Wh/kg while jet fuel has a specific energy of 12000 Wh/kg. That means putting a bigger battery in the plane is not a solution either because of the weight. The limited capacity of energy stored by batteries makes it important for electric aircraft to be as efficient as possible. The vast majority of existing prototypes and concepts

for electric aircraft are using a propeller connected to an electric engine as the propulsion system. For electric aircraft, the noise generated by the propeller is dominant since an electric motor is generally not as loud as a traditional combustion engine. To meet the noise requirements for future aircraft, it is then necessary to reduce the propeller's noise radiation. There are many different design parameters that affect the noise radiation of a propeller, and getting a full understanding of their importance is critical to model an efficient propeller that does not create a lot of noise.

1.3 Purpose

The main objective of this project is to study how different parameters effect aerodynamic performance and noise emissions from a propeller. These effects will be investigated for the aircraft model ES-19 which is under development. To accomplish this the in-house program *OptoProp* will be used to design the propeller blades for an open rotor aircraft engine. The program will also be expanded to allow for calculation of noise radiation which is sought to be minimised. These results will finally be used to propose guidelines to follow when designing low-noise propellers. To determine the effects on noise radiation for different propeller parameters, such as *blade count*, *blade diameter* or *rotational speed* MATLAB programs will be created and implemented to work with *OptoProp*.

1.4 Limitations

The main constraint of this project is the time limit in which it has to be completed. The project duration is restricted from January to the end of May and the amount of time that each student can invest is limited. Therefore the scope needs to be narrowed down in order to ensure that it is completed in time. The project is also limited to be a theoretical study only. That means there will be no real life testing conducted to verify the results from the study, instead the result will be validated by comparing results to known studies.

The conducted studies will be constricted to a specific number of propeller parameters, this is done in order to save time. The study is also based on the developing aircraft model (ES-19) and no other models will be taken into account during the time of the project.

1.5 Outline

This section covers the overall structure of the thesis and explains each chapter and its contents.

Chapter 2 covers the theoretical background behind the design of the propeller and implementation in MATLAB. The validation case for propeller design is illustrated in this chapter illustrating the reliability of the software. The theoretical background describes Adkins design theory of minimum induced loss and explains the algorithm for *OptoProp*. This chapter also explains the creation of a 3D model based on the output data from *OptoProp*. Theoretical description for the creation of the 3D modeling and visual pictures illustrating the geometry are key points under this section. The thesis then moves onto chapter 3 covering the parameter research which is a study conducted to better understand how different parameters affect the general efficiency of the propeller. This chapter covers how the parameters work individually and collectively resulting in new data. There was also a smaller study conducted covering the effect from altering the amount of propellers on the airplane.

Chapter 4 describes existing theory used to perform acoustic calculations for noise evaluation. This theory is used to develop MATLAB programs which are validated before being used to study the effects the parameters have on the generated noise, similarly to chapter 3. The studies are initially conducted for a single propeller before investigating the noise generated by multiple propellers and their distribution.

Chapter 5 contains the conclusions of the thesis. First, it describes the conclusions drawn from the propeller design and then from the acoustic studies. Lastly, a correlation between both parts is formulated to provide guidelines for an optimal low-noise design. Chapter 6 contains an ethical analysis of the methodology and the results of the project, and chapter 7 describes which types of propellers that could have been studied if the thesis had a larger time frame. It also provides a suggestion on work that can be done in the future.

2

Propeller Design

This chapter covers the theoretical methodology for the design of the propeller using Adkins design theory. The formulations and definitions are the foundation of the parameter study and 3D modeling. Adkins design theory is described in multiple earlier works such as Adkins, Liebeck [7] and Patrao [8], and for this chapter it will be adapted for the study of alternated parameters. The verification case and creation of the baseline propeller is also detailed in this chapter.

2.1 Design Methodology

This section describes the propeller design methodology created by Adkins and Liebeck [7], illustrating a method to iteratively design a high efficient propeller. Based on a specific amount of inputs, the methodology has been implemented in a MATLAB environment, which algorithm will be explained.

2.1.1 Adkins Design Theory

Adkins design theory includes a propeller design procedure which generates a propeller with minimum induced loss, creating a highly efficient propeller design.

2.1.1.1 Momentum Equations

Based on Adkins and Liebeck [7] momentum equations, consider a fluid with the mass $\mathrm{d}m$ moving towards the propeller disc in an annular tube stream with the velocity V. Once arriving at the disc the velocity increases to $V(1+a)$ as a represents the axial interference factor, this can also be seen in figure 2.1(a). Once at the disc the fluid lies within the annular volume $2\pi r \mathrm{d}r$ and the flow in the radial direction is neglected, this allows the mass rate per unit area flowing through the disc to be written as $2\pi r \rho V(1 + a)$. When the fluid flows downstream and reaches the wake, the speed is increased to $V(1 + b)$, where b is represented by the axial slipstream factor. Standard momentum theory defines b as precisely $2a$ and even though general momentum theory defines b as approximately $2a$ it is assumed for this methodology that $b = 2a$. This implies that the general change in momentum for an element is $2VaF\mathrm{d}m$, where F is defined as the momentum loss factor and corrects the neglecting of the radial flow. Now the thrust per unit radius T' may be expressed as

$$T' = \frac{dT}{dr} = 2\pi r \rho V (1+a)(2VaF) \tag{2.1}$$

The torque per unit radius Q' can be expressed as

$$\frac{Q'}{r} = 2\pi r \rho V (1+a)(2\Omega r a' F) \tag{2.2}$$

This definition (2.2) relies on the same arguments made for the sectional unit thrust where Ω is defined as the propellers angular velocity and a' is the rotational interference factor which can also be seen in figure 2.1(a).

2.1.1.2   Wake Equations

According to Adkins and Liebeck [7] the helical wake is modelled as a vortex sheet, by using figure 2.1(a) the tangential velocity far downstream is expressed as

$$w_t = w_n \sin \phi = v' \sin \phi \cos \phi \tag{2.3}$$

Where v' is defined as the displacement velocity and w_t is the tangential velocity within the vortex.
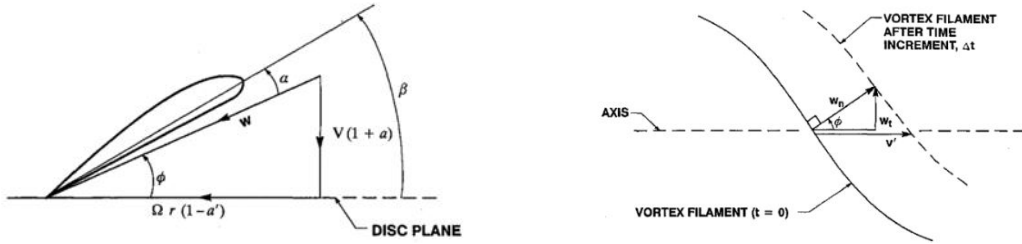
(a) Blade section with flow angle and induced velocities. Source: Adkins and Liebeck [7].

(b) Propeller wake far downstream. Source: Adkins and Liebeck [7].

Figure 2.1: Illustration of a blade element and the definition of v'.

Combining equation (2.3) and (2.5), implementing formulation (2.4) which describes the circulation in the annulus, the final expression for the circulation G can be defined as

$$\zeta = \frac{v'}{V} \tag{2.4}$$

$$B\Gamma = 2\pi r F w_t \implies \Gamma = \frac{2\pi V^2 \zeta G}{B\Omega} \tag{2.5}$$

$$G = Fx \cos \phi \sin \phi \tag{2.6}$$

$$x = \frac{\Omega r}{V} \tag{2.7}$$

There are forces affecting the propeller during flight and using figure 2.2 the definitions for T' and Q' can be rewritten. This can be seen in equation (2.8) and (2.9) where ϵ is the drag-to-lift ratio for each blade element. In figure 2.2, L' is the lift force per unit radius and D' is the drag force per unit radius. The angles are defined as α being the angle of attack, β representing the blade twist angle and lastly, ϕ is the flow angle.
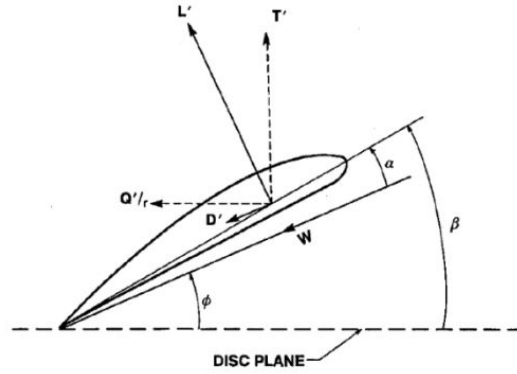
Figure 2.2: Blade element with forces, Source: Adkins and Liebeck [7].

$$T' = L' \cos \phi - D' \sin \phi = L' \cos \phi (1 - \epsilon \tan \phi) \tag{2.8}$$

$$\frac{Q'}{r} = L' \sin \phi + D' \cos \phi = L' \sin \phi \left(1 + \frac{\epsilon}{\tan \phi} \right) \tag{2.9}$$

$$L' = \frac{\mathrm{d}L}{\mathrm{d}r} = B \rho W \Gamma \tag{2.10}$$

2.1.1.3 Minimum Energy Loss

From this, the interference factors a and a' can be formulated by putting equations (2.1), (2.2) equal to (2.8) and (2.9). The axial and tangential interference factors can now be defined as

$$a = \frac{\zeta}{2} \cos^2 \phi (1 - \epsilon \tan \phi) \tag{2.11}$$

$$a' = \frac{\zeta}{2x} \sin \phi \cos \phi \left(1 + \frac{\epsilon}{\tan \phi} \right) \tag{2.12}$$

Where equations (2.6) and (2.5) have been used to express the lift force per unit radius L' in terms of ζ. Equations (2.11) and (2.12) combined with the geometry in figure 2.1 leads to the following relation.

$$\tan \phi = \frac{(1 + \frac{\zeta}{2})}{x} = \frac{(1 + \frac{\zeta}{2}) \lambda}{\xi} \tag{2.13}$$

In this equation ξ varies from ξ_0 at the hub of the propeller to the edge of the disc.

2.1.1.4 Constraint Equations

For Adkins design theory the process is similar to that of Larrabees described by Patrao [8] and therefore the formulation will not be written in great detail for this section. The principle is that the design of the propeller is constrained by setting a static torque or power, for this study an arbitrary thrust will be specified.

$$\xi = \frac{I_1}{2I_2}\left(1 + \sqrt{1 - \frac{4I_2 T_c}{I_1^2}}\right) \tag{2.14}$$

$$\frac{\mathrm{d}I_1}{\mathrm{d}\xi} = 4\xi G(1 - \epsilon \tan\phi) \qquad \frac{\mathrm{d}I_2}{\mathrm{d}\xi} = \frac{\lambda}{2\xi}\frac{\mathrm{d}I_1}{\mathrm{d}\xi}\left(1 + \frac{\epsilon}{\tan\phi}\right)\sin\phi\cos\phi \tag{2.15}$$

The idea is that by integrating the equations in (2.15), the velocity displacement ratio can be found.

2.1.1.5 Blade Geometry

The blade is divided into separate individual elements with the length $\mathrm{d}r$. For one random element let C_l be the local lift coefficient and c is the chord. This allows the lift per unit radius for one blade to be defined as

$$\frac{\rho W^2 c C_l}{2} = \rho W \Gamma \tag{2.16}$$

This formulation directly translates to the following definition by using equation (2.5).

$$Wc = \frac{4\pi\lambda G V R\zeta}{C_l B} \tag{2.17}$$

2.1.1.6 Prandtl Tip Loss Factor

Based on the formulations described by Adkins and Liebeck [7], the Prandtl tip loss factor is described as

$$F = \frac{2}{\pi}\arccos(e^{-f}) \qquad f = \frac{B}{2}(1-\xi)\frac{1}{\sin\phi_T} \qquad \phi_T = \arctan(\lambda(1 + \frac{\zeta}{2})) \tag{2.18}$$

2.1.2 Implementation in MATLAB

Adkins theory has been implemented into MATLAB taking benefit of its iterative property. This allows the user to easily change and alter inputs, resulting in the most efficient version of the propeller based on the theoretical background. The algorithm uses Adkins design theory as *OptoProp* but before initiation there are a couple of parameters that has to be set. These include blade count, coefficient of thrust, design lift distribution, hub radius, axial velocity, rotational velocity and lastly the diameter of the propeller.

The layout of the design algorithm is based on the one found under section 3.3.8 in [8] and its methodology is listed as:

1. Initial guess for ζ
2. Calculate:
    (a) The Prandtl tip loss factor, equation (2.18)
    (b) The flow angle for each radial position with equation (2.13)
    (c) The G function with equation (2.6)
    (d) The product of the chord and total velocity W, used to calculate Reynolds number.
3. Calculate angle of attack α and coefficient of drag c_d from airfoil data which allows calculation of $\epsilon = \frac{c_d}{c_l}$
4. Calculate a' and a
5. Calculate chord and blade angle β
6. Integrate equation (2.15) and solve equation (2.14)
7. Repeat from step 2 until ξ converges below set limit
8. Calculate $\frac{\mathrm{d}Q}{\mathrm{d}r}$ and $\frac{\mathrm{d}T}{\mathrm{d}r}$ and integrate, this gives the sought thrust, torque and efficiency

2.2 Validation

The initial step of the propeller design was to verify the reliability of *OptoProp*, by comparing calculated results to already established data, using identical inputs. The verification was done to confirm that the program does not contain initial errors that may alter the results from the calculations. The thrust, power and efficiency were compared to visualise the error of the program, this can be seen in table 2.1. The verification case by Patrao [8] also included a graph of the sectional thrust profile, these were also compared to further ensure the accuracy of *OptoProp*. The calculations for the validation used Adkins design theories described in chapter 2.1.1, using an eight bladed propeller called GPS621.

Table 2.1: Data comparison between validation case (GPS621) and *OptoProp*.

	CFD	*OptoProp*	Error
Thrust, [N]	333.2	334.9	0.51%
Power, [kW]	93.35	96.6	3.5%
Efficiency, [%]	79.38	77.1	2.9%
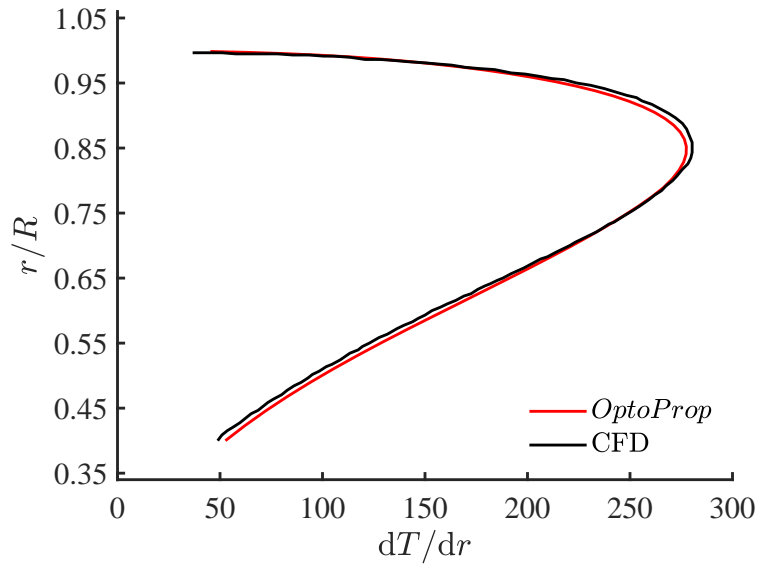
Figure 2.3: Sectional thrust comparison of the computed result with reference data (input data from section 5.6 in Patrao [8]).

The computed data was found satisfactory due to its similarity with the already calculated case by Patrao [8], this implies that *OptoProp* is accurate enough to continue the parameter study and no adjustments has to be made in the program.

2.3 Baseline Propeller

This section describes the creation of the baseline propeller, evaluating its aerodynamic performance. The baseline propeller is used as the reference case that all other propellers will be compared against. The configuration and individual parameters used to create the propeller are presented in table 2.4.

2.3.1 Thrust Derivation

The theoretical background of Adkins and Liebeck [7], implies that an optimal design for a propeller is created at a static thrust. This entails that a specific thrust needs to be derived as a design constraint. For this study the airplane data is based on the turboprop driven airplane Beechcraft 1900D, 19 passenger aircraft. The airplane specifications this process is based upon can be found in table 2.2. For conventional airplanes such as Beechcraft 1900D the weight varies during flight due to fuel consumption, since this study is focuses on electric aircraft the weight is assumed to be constant.

Table 2.2: Performance and specifications of the Beechcraft 1900D.

Maximum Takeoff Weight	7766	kg
Operational Empty Weight	4847	kg
Fuel	687	kg
Payload	1938	kg
Crew/Passengers	2/19	-
Reference Area	29.08	m^2
Aspect Ratio	10.41	-
Span	17.64	m

The process of calculating the sought cruise thrust is based on the process introduced in Huang, Yao [9]. It is known that the desired thrust is equivalent to the drag of the aircraft because of force equilibrium in the horizontal plane.

$$T_c = D_c \tag{2.19}$$

This total drag may then be formulated as

$$D_c = \frac{1}{2}\rho V^2 C_d S \tag{2.20}$$

The variables ρ and V are fluid properties at cruise speed formulated from table 2.3. C_D represents the coefficient of drag calculated in equation (2.21).

$$C_D = C_{D0} + \frac{C_L^2}{\pi e \lambda} \tag{2.21}$$

The evaluation of C_{D0} and e can be found in [9] where e is described as the Oswald efficiency and C_{D0} represents the zero-lift drag coefficient. C_L is the coefficient of lift which can be calculated through force equilibrium in the vertical plane.

$$C_L = \frac{2W_{to}}{\rho V^2 S} \tag{2.22}$$

This study relies on the cruise thrust calculated from this methodology where the properties of the electric aircraft are represented by table 2.2. The fluid properties used in the equations are based on the operational conditions of the airplane found in table 2.3. These flight conditions will be used throughout this study as the standard specifications. From this process the thrust could be evaluated during flight and its respective coefficient of thrust can be found in table 2.3.

Table 2.3: Operational flight conditions of the propeller.

Flight Mach number	0.35	-
Flight altitude	5150.62	m
Hub tip ratio	0.25	-
Advance ratio	1.4	-
Coefficient of thrust	0.137	-

2.3.2 Configuration and Performances

The baseline propeller is designed for maximum efficiency using *OptoOrop* and the design procedure is thus based on Adkins Design Theory in chapter 2.1.1. The Parameters specified as input for *OptoProp* when running the baseline case are listed in table 2.4.

Table 2.4: Parameter values used to create baseline propeller.

Blade count	6	-
Diameter	2.2	m
Flight altitude	5150.62	m
Rotation speed	2200	RPM
Coefficient of thrust	0.137	-

The parameters required to design the propeller are camber, chord and thickness and are all extracted from *OptoProp*. The distribution of these parameters over the dimensionless radius is shown in figure 2.4-2.7.
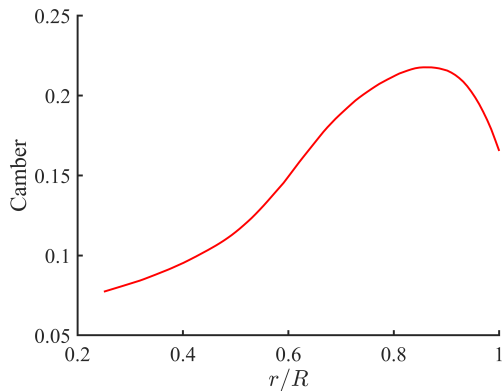
Figure 2.4: Camber line plotted against dimensionless radius.
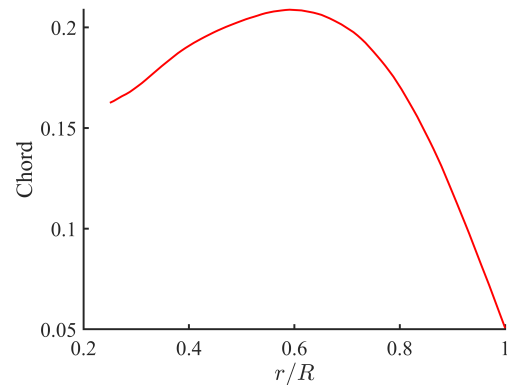
Figure 2.5: Chord line plotted against dimensionless radius.
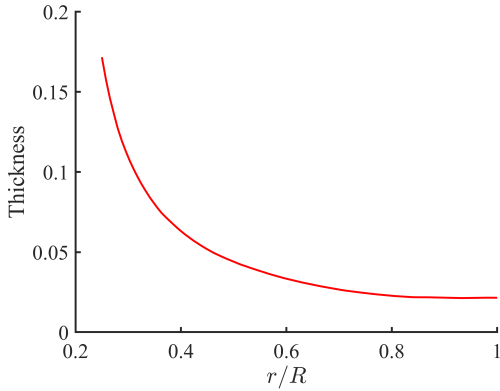
Figure 2.6: Thickness plotted as percentage of the chord line.
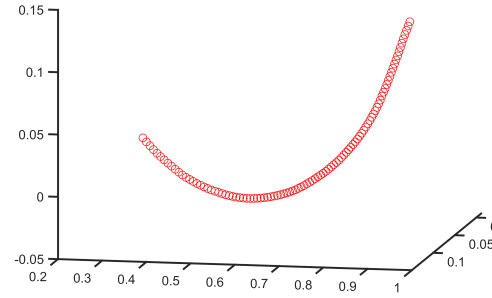
Figure 2.7: Stacking line plotted against dimensionless radius.

OptoProp also evaluates the performance of the designed propeller and the results are presented in table 2.5.

Table 2.5: Aerodynamic performance of baseline propeller calculated using *Opto-Prop*.

Coefficient of thrust	0.137	-
Coefficient of power	0.2158	-
Efficiency	88.0193	%
Thrust	3125.4	N
Power	397.04	kW
Disc loading	82.0331	kW/m^2

2.3.2.1 Generation of Blade Geometry

The purpose of this section is to explain how to visualize the design of a propeller optimized in *OptoProp*. The data needed to specify the propeller geometry is chord line, camber line, thickness, blade angle and stacking line and can all be extracted as data from *OptoProp*. The geometry of a propeller blade is described by number of airfoils which can be described as a 2D slice of the propeller capturing the shape of the propeller cross section. To create the propeller multiple airfoils are then stacked in a special way.

The airfoils used in this project are of the NACA16 family and are suitable for designing high speed propellers. With the camber line, chord line and thickness known, the shape of the airfoils can be calculated analytically using equations (2.23), (2.24) and (2.25) [9].

$$y_1 = 0.01\frac{t}{c}(0.989865x_1^{0.5} - 0.23925x_1 - 0.041x_1^2 - 0.5594x_1^3) \qquad (2.23)$$

$$y_2 = 0.01\frac{t}{c}[0.01 + 0.2325(1 - x_2) - 3.42(1 - x_2)^2 + 1.46(1 - x_2)^3] \qquad (2.24)$$

$$y_c = -0.079577c_l[x \ln x + (1-x)\ln(1-x)] \tag{2.25}$$

In the first two equations, y_1 and y_2 are the lengths of the chord on respective sides of the point of maximum thickness measured in the direction normal to the camber line. $\frac{t}{c}$ is the relation between thickness and chord in percentage. In equation (2.25), y_c is the distance between the chord and camber line measured vertical and C_L is the lift coefficient [9]. These equations are implemented in *OptoProp* in the function *CoordinatesNACA16*. The function takes camber, chord and thickness as input to compute the airfoil shape and returns a matrix of dimensions $2n$ x 2 where n is the number of points along the upper camber and lower camber respectively.
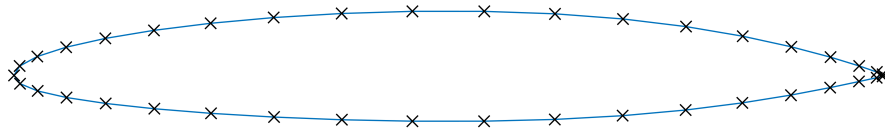
Figure 2.8: Single airfoil with 20 points on upper and lower camber respectively.

$$airfoil = \begin{bmatrix} x_1 & y_1 \\ x_2 & y_2 \\ \vdots & \vdots \\ x_{2n} & y_{2n} \end{bmatrix} \tag{2.26}$$

A propeller blade is made up of multiple airfoils distributed along the radius of the propeller. By computing all the airfoils along the radius the blade geometry with the desired shape can be create by stacking the airfoils according to the stacking line and blade angle. The process of stacking the airfoils is described below.

First the blade angle β is added to the airfoil. The airfoil is moved to have the center airfoil coincide with the origin by adding half of the chord length to the x-coordinate of the airfoil. The airfoil is already centered in the y-direction. Each of the points in the airfoil is then rotated around the z-axis with respect to the blade angle β.

$$airfoil_{centered} = \begin{bmatrix} x_1 + \frac{chordlength}{2} & y_1 \\ x_2 + \frac{chordlength}{2} & y_2 \\ \vdots & \vdots \\ x_{2n} + \frac{chordlength}{2} & y_{2n} \end{bmatrix} = \begin{bmatrix} x_{1,centered} & y_1 \\ x_{2,centered} & y_2 \\ \vdots & \vdots \\ x_{2n,centered} & y_{2n} \end{bmatrix} \tag{2.27}$$

$$airfoil_{rotated} = \begin{bmatrix} x_{1,centered}\cos\beta - y_1\sin\beta & y_1\cos\beta + x_{1,centered}\sin\beta \\ x_{2,centered}\cos\beta - y_2\sin\beta & y_2\cos\beta + x_{2,centered}\sin\beta \\ \vdots & \vdots \\ x_{2n,centered}\cos\beta - y_2 n\sin\beta & y_{2n}\cos\beta + x_{2n,centered}\sin\beta \end{bmatrix} =$$

$$
\begin{bmatrix}
x_{1,rotated} & y_{1,rotated} \\
x_{2,rotated} & y_{1,rotated} \\
\vdots & \vdots \\
x_{2n,rotated} & y_{2n,rotated}
\end{bmatrix}
\tag{2.28}
$$

The stacking line is the center line of the propeller blade and is used to properly stack the airfoil. The airfoil is placed to have the center coincide with the stacking line and the stacking line also distributes the airfoils along the radius of the propeller.
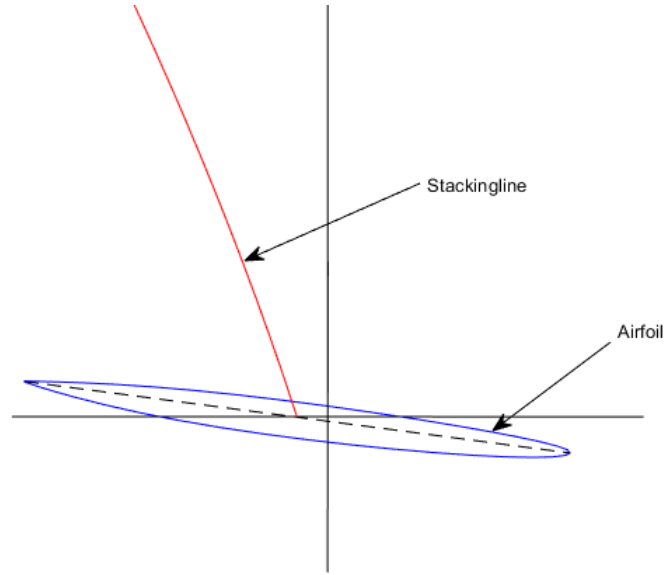
Figure 2.9: Correctly positioned airfoil.

$$
airfoil =
\begin{bmatrix}
x_{1,rotated} + x_{stacking} & y_{1,rotated} + y_{stacking} & z_{stacking} \\
x_{2,rotated} + x_{stacking} & y_{1,rotated} + y_{stacking} & z_{stacking} \\
\vdots & \vdots & \vdots \\
x_{2n,rotated} + x_{stacking} & y_{2n,rotated} + y_{stacking}, z_{stacking}
\end{bmatrix}
\tag{2.29}
$$

By repeating this process for all the airfoils the blade geometry is obtained. The stacked geometry of the baseline propeller blade is visualized in figure 2.10 using a 3D plot in MATLAB. To create a better model of the baseline propeller the co-ordinates of the stacked airfoils can be imported into CAD software, for creating the baseline propeller CATIA V5 was used. To import the coordinates a MATLAB script was created, the script stacks the airfoils as described previous and saves the stacked coordinates as an excel document with the required delimiters between each airfoil. Using a macro for excel the coordinates were imported to CATIA V5 and a surface geometry was created.
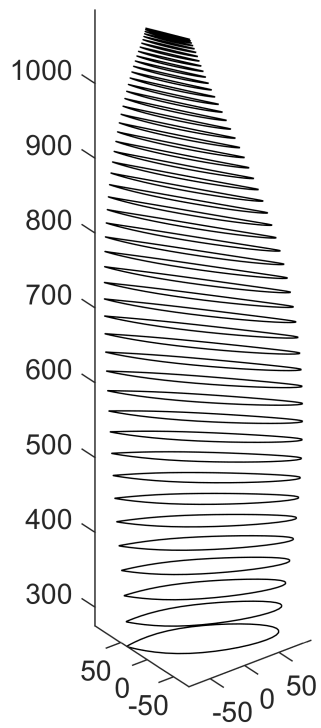
Figure 2.10: Stacked airfoils.

Figure 2.11: 3D model of baseline propeller created in CATIA V5.

3

Research on Various Propeller Parameters

This chapter covers the parameter research conducted to study how altering propeller parameters affect the efficiency and torque. This includes a single parameter, multiple parameter and multiple propeller study.

3.1   Single Parameter

Utilizing *OptoProp* and its implemented formulas, the parameters connection with efficiency, coefficient of lift and torque could be calculated. Firstly, the cruise thrust was calculated using the methodology described in section 2.3.1, this static thrust is maintained throughout the study as a constant variable.

The study is based on altering specific propeller parameters and documenting the output from *OptoProp*. To simplify the analysis of the results they have been visualised as graphs and tables. The main parameters that are studied are found in table 3.1, where each parameter consists of five separate values.

Table 3.1: Propeller parameter values used in the study.

Rotation speed	1800	2000	**2200**	2300	2400
Blade number	2	3	4	**6**	8
Diameter	1.5	2.0	**2.2**	2.3	2.4

The first study was conducted by altering one of the parameters in table 3.1 while maintaining the other two parameters as for the baseline propeller. This provided data on how each individual parameter changes the efficiency, torque and coefficient of lift. Important to note is that the thrust relies on the values of the parameters implying that when they are changed the thrust also changes. This was solved by for each test, changing the coefficient of thrust in order to maintain the thrust at a constant value.

(a) Illustration of how change in the angular velocity affects the propeller efficiency
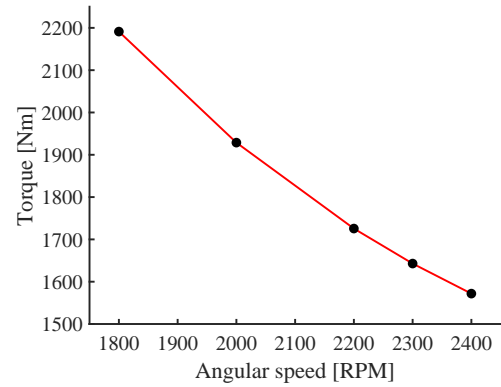
(b) Visualisation of how change in angular speed affects the generated torque.

Figure 3.1: Illustration of how angular speed affects the overall efficiency and torque of the propeller.
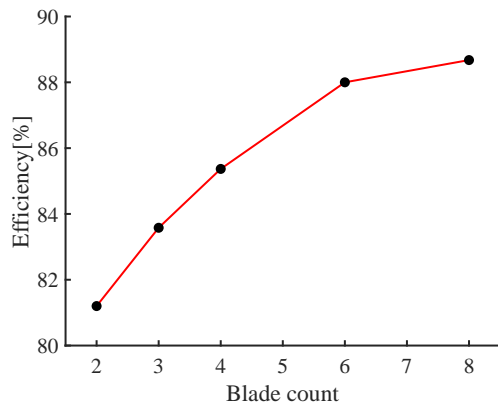
(a) Connection between blade count and propeller efficiency.
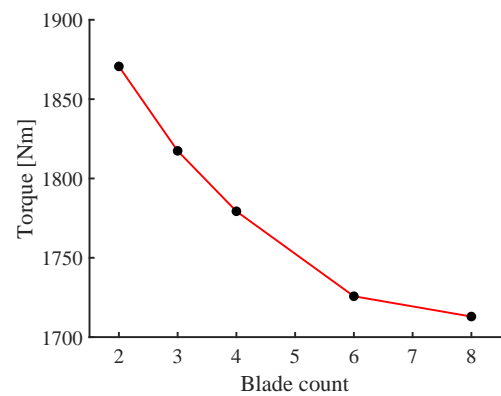
(b) Visualisation of how change in torque is affected by the number of blades.

Figure 3.2: Illustration of how blade count affects the overall efficiency and torque of the propeller.
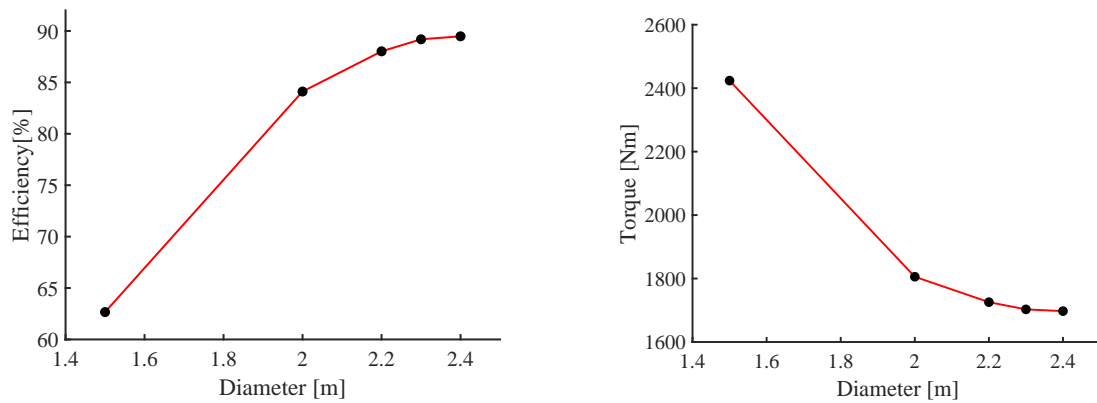
(a) Illustration of how change of diameter alters the propeller efficiency.

(b) How change in propeller diameter affects the generated torque.

Figure 3.3: Illustration of how diameter affects the overall efficiency and torque of the aircraft propeller.

There is a trend from these tests showing that the efficiency increases with increased parameter values, although the growth rate decreases. This implies that for single parameters the highest values creates the highest efficiency for the propeller. The torque shows a different trend falling in value as the parameter values increases.

For the second test there was also an interest in studying how the lift coefficient distribution changes while alternating the propeller parameters. This was done by dividing the airfoil into individual sections and then calculate the coefficient of lift for each section. *OptoProp* calculates the distribution along the airfoil and the result from these calculations have been illustrated in figures 3.4, 3.5 and 3.6.
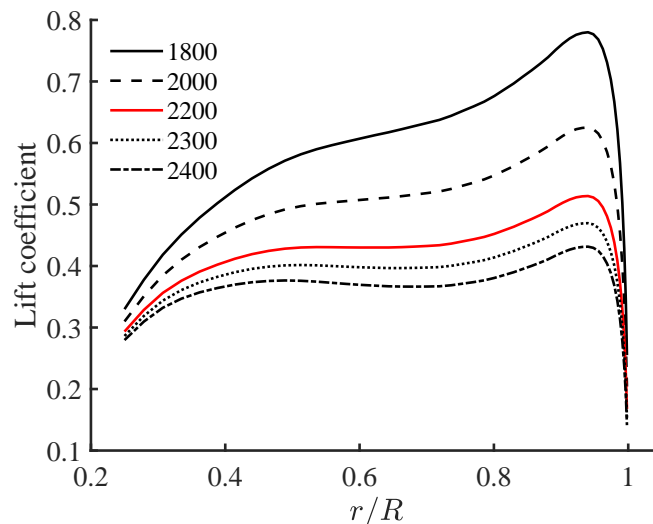
Figure 3.4: Distribution of lift coefficient along nondimensional radius with changing angular speeds.

19
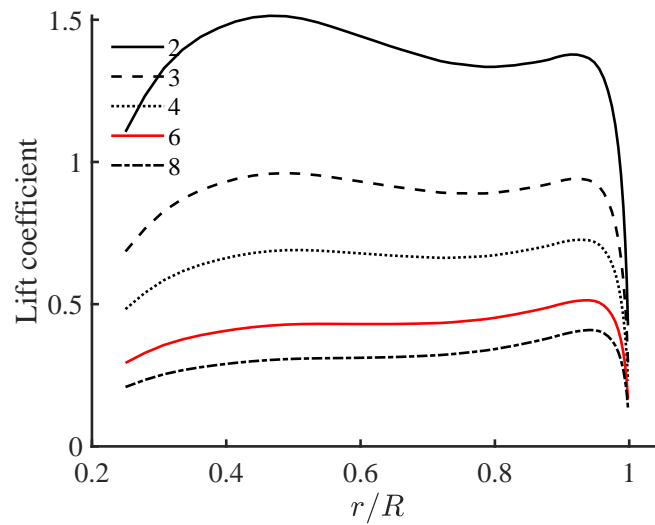
Figure 3.5: Distribution of lift coefficient along nondimensional radius with changing number of blades.
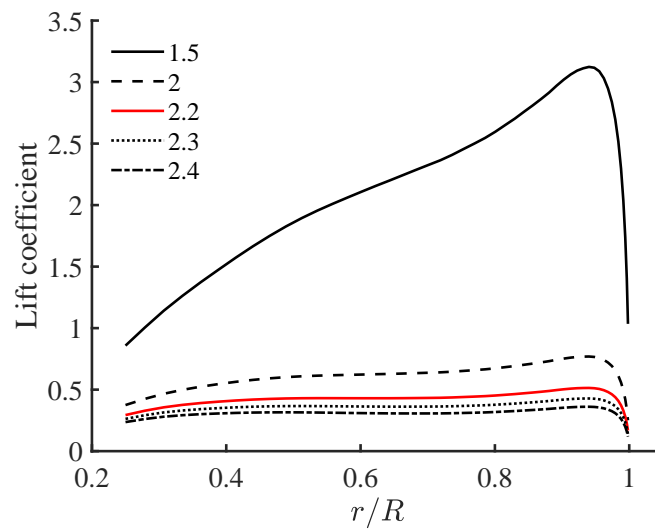
Figure 3.6: Distribution of lift coefficient along nondimensional radius with changing diameters.

For the lift coefficient distribution there is a trend which shows that it increases up to a specific point towards the end of the blade, after which is rapidly falls. For the diameter however, which can be seen in figure 3.6, the highest lift is found at the beginning of the propeller blade at a non dimensional radius of around 0.42. The results also show that the coefficient of lift is increased as the individual parameters are lowered in value.

3.2 Multiple Parameters

In the previous section only one parameter was altered for each test but for this study the connection between changing both the blade count and angular velocity will be studied. This was done by testing five different angular velocities for each number of blades found in table 3.1. The result of this study can be found in figure 3.7 where the y-axis is represented by the efficiency and torque, as in the previous tests and the x-axis is the helical tip Mach number. The formulation for this was provided by Roskam, Lan [11] which describes the relation between the forward speed U, rotational velocity n and tip speed U_{tip}.

$$U_{tip} = \sqrt{(\pi Dn)^2 + U^2} \tag{3.1}$$

This equation was then rewritten in terms of Mach number which provided the sought helical tip Mach number. This was done by dividing equation 3.2 with the speed of sound.

$$M_{tip} = \sqrt{\left(\frac{\pi Dn}{a}\right)^2 + M^2} \tag{3.2}$$
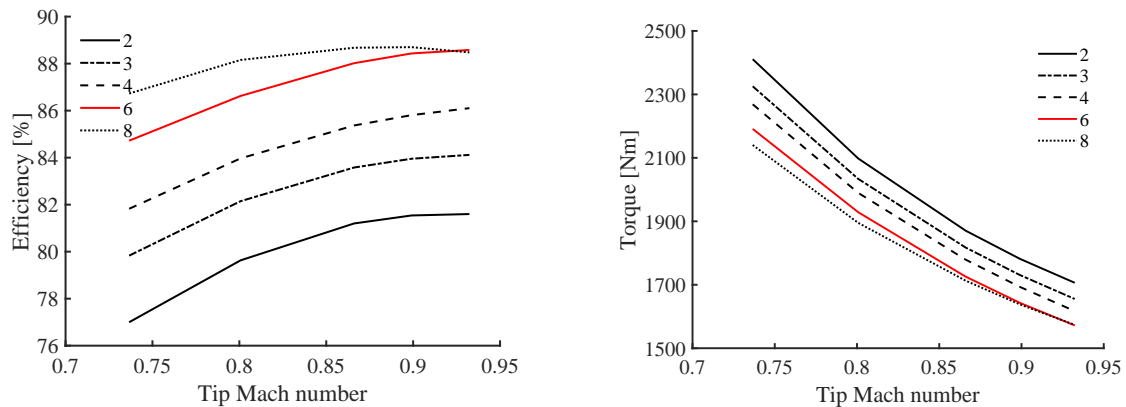
(a) Efficiency change compared to helical tip Mach number.

(b) Torque compared to helical tip Mach number.

Figure 3.7: The propeller efficiency and torque, visualised for different tip Mach numbers and blade counts, each line represent different tip Mach numbers with the same number of blades.

The same trend as in the previous study can be found where increasing the parameters generally transfer into an increased efficiency. The higher angular speed and larger number of blades generally lead to a high propeller efficiency. However, there is a slight dip for eight blades at the highest angular speed which shows that at some point the trend of increased efficiency may change and lead to a lower value. This implies that simply maximising the individual values does not translate to the most efficient propeller.

3.3 Multiple Propellers

For an electric aircraft there is a possibility to alter the number of propellers connected to the aircraft. The way this study was conducted was by taking the static thrust and divide it by the amount of propellers being used. The new thrust was then calculated for one propeller and then the efficiency, torque etc. was documented. The results of this study can be found in table 3.2 where each column represents a different number of propellers. The standardized parameters are used throughout this study which can be found in table 3.1 as the values in bold.

Table 3.2: Data from calculations made on changing number of propellers.

Number of propellers	2	3	4	6	-
Efficiency	88.02	90.53	90.86	89.67	%
Coefficient of thrust	0.137	0.091	0.068	0.046	-
Torque	1725.74	1118.49	835.83	564.62	Nm

The following figures display the multiple propellers setups used during these studies, with figure 3.8(a) illustrating how the seven different propellers are positioned on the airplane. Figure 3.8(b) shows which propeller position is used for the different configurations, for example the three propeller configuration have the propellers placed in position 1, 2 and 3.

(a) Distance between propellers.

(b) Propellers numbers.
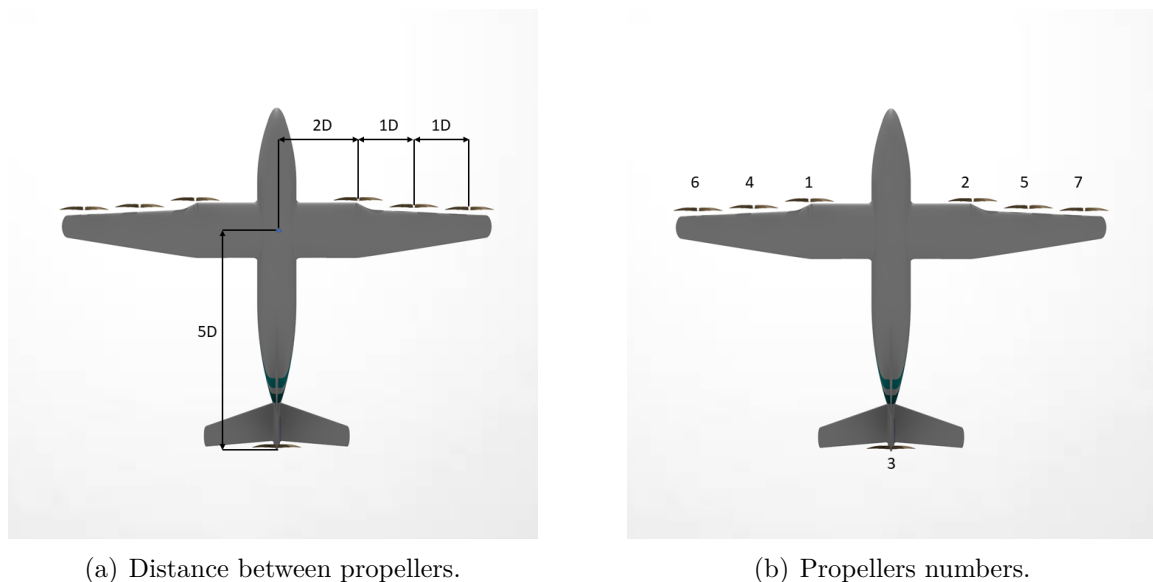
Figure 3.8: Schematic of propeller distributions. Source for aircraft model: [12].

4
Acoustic Studies

This chapter will introduce the necessary acoustic theory and the methods that were used to calculate the sound pressure levels (SPLs) of different propellers. The verification of the developed programs will also be discussed. Once verified, the SPLs for the baseline propeller model were calculated and the effects of each parameter, multiple propellers and their distribution were all studied.

4.1 Acoustic Theory

The acoustic formulas used in this chapter are largely based on work done by Garrick and Watkins [6]. In their work, there are equations describing the SPL from propellers for two cases. The first instance is the near field, which is calculated at a radius in the order of a few propeller diameters around the propeller. The second case is the far field, where far is considered to be in the magnitude of hundreds of propeller diameters.

These calculations use some assumptions, for example that the noise is mainly generated by the thrust and torque experienced by the propeller. Another simplification is done by calculating a so-called effective radius $R_e = 0.8D/2$, as a function of the propeller diameter D. This allows the noise to be calculated as originating from an annular ring where the forces are concentrated, the coordinates of which can be introduced as (x_l, y_l, z_l). The propeller is considered to be moving uniformly with a constant velocity along the positive x-axis. The coordinates of the observers, or field points, are called (x, y, z) and can be converted from Cartesian coordinates to polar or spherical coordinates to calculate the SPLs around a propeller.

Now the pressure levels associated with the forces on the propeller can be derived. Because of the assumption that the forces are concentrated on an annular ring there is no integration with respects to the propeller radius necessary. This also means that the loading coordinates, the source of the noise, have the values $x_l = 0$, $y_l = R_e \cos\theta$ and $z_l = R_e \sin\theta$, where θ is the polar angle for the plane of rotation. The following equations originate from the thrust and torque, denoted by T and Q respectively.

$$p_T' = \frac{e^{i\omega t}}{4\pi^2} \int_0^{2\pi} T\left(\frac{ikM}{\beta^2} + \frac{ikx}{\beta^2 S} + \frac{x}{S^2}\right) \frac{e^{-i(mB\theta + k\sigma)}}{S} \, \mathrm{d}\theta \qquad (4.1)$$

$$p_Q' = -\frac{e^{i\omega t}}{4\pi^2} \int_0^{2\pi} \frac{Q}{R_e^2} imB \frac{e^{-i(mB\theta + k\sigma)}}{S} \, \mathrm{d}\theta \qquad (4.2)$$

$$S = \sqrt{(x - x_l)^2 + \beta^2[(y - y_l)^2 + (z - z_l)^2]} \tag{4.3}$$

$$\sigma = \frac{M(x - x_l) + S}{\beta^2} \tag{4.4}$$

$$\beta = \sqrt{1 - M^2} \tag{4.5}$$

Here m refers to the harmonic number, B blade count, M forward-speed Mach number and $k = \Omega/c_0$ is the wave number, where c_0 refers to the speed of sound and Ω the angular velocity. θ is the polar angle in the plane of rotation for the propeller and also the variable of integration from 0 to 2π. T and Q are the propeller thrust and propeller torque, respectively. These forces have previously been calculated as described in chapter 2.1.2.

Then, the root-mean-square pressure p'_{rms} can be calculated from equations (4.1) and (4.2) through the following formula.

$$p'_{rms} = \frac{\sqrt{2}}{2} |p'| = \frac{\sqrt{2}}{2} \left| p'_T + p'_Q \right|$$
$$= \frac{\sqrt{2}}{8\pi^2} (A^2 + B^2)^{1/2} \tag{4.6}$$

Here, equations (4.1) and (4.2) have been reformulated in favor of equation (4.6) which is reliant on A and B, equations (4.7) and (4.8) below. This can be done when evaluating the SPLs from only one propeller to avoid the calculations dependant on time, t.

$$A = \int_0^{2\pi} \left\{ \frac{Tx}{S^2} \sin mB\theta + k\sigma + \left[T\frac{k}{\beta^2}\left(M + \frac{x}{S}\right) - Q\frac{mB}{R_e^2} \right] \sin(mB\theta + k\sigma) \right\} \frac{\mathrm{d}\theta}{S} \tag{4.7}$$

$$B = \int_0^{2\pi} \left\{ -\frac{Tx}{S^2}\sin(mB\theta + k\sigma) + \left[T\frac{k}{\beta^2}\left(M + \frac{x}{S}\right) - Q\frac{mB}{R_e^2} \right] \cos mB\theta + k\sigma \right\} \frac{\mathrm{d}\theta}{S} \tag{4.8}$$

The next step is to formulate the equations for the SPL in the far field. Just like with the near field, the far field pressure levels are also almost exclusively generated by the thrust and torque. These equations are as follows.

$$p'_T = T\frac{e^{i\omega t}}{2\pi S_0}i^{mB}e^{-i\frac{k}{\beta^2}(S_0 + Mx)}\frac{ik}{\beta^2}\left(M + \frac{x}{S_0}\right)J_{mB}\left(\frac{kzR_e}{S_0}\right) \tag{4.9}$$

$$p'_Q = -\frac{Q}{R_e^2}\frac{e^{i\omega t}}{2\pi S_0}i^{mB+1}mBe^{-i\frac{k}{\beta^2}(S_0 + Mx)}J_{mB}\left(\frac{kzR_e}{S_0}\right) \tag{4.10}$$

$$S_0 = \sqrt{x^2 + \beta^2 z^2} \tag{4.11}$$

In these equations S_0 serves the same purpose as S from before, the difference being that z denotes the altitude of the propeller when calculating the SPL along the x-axis. The fundamental frequency, ω_1 is also introduced which is the product of the angular velocity and the blade count, $\omega_1 = B\Omega$. J_{mB} refers to the Bessel function of the first kind.

Also similarly to the near field, equations (4.9) and (4.10) combine into the root-mean-square pressure p'_{rms} through the following equation.

$$
\begin{aligned}
p'_{rms} &= \frac{\sqrt{2}}{2} \left| p'_T + p'_Q \right| \\
&= \frac{m\omega_1}{2\sqrt{2}\pi c_0 S_0} \left| T \left(M + \frac{x}{S_0} \right) \frac{1}{\beta^2} - Q \frac{Bc_0}{\omega_1 R_e^2} \right| J_{mB} \left(\frac{kzR_e}{S_0} \right)
\end{aligned} \tag{4.12}
$$

Here the standalone thrust and torque pressure levels have also been reformulated into an equation that omits the dependency of time. Note that equation (4.12) should only be used if the SPL is to be calculated for a single propeller.

To efficiently calculate the SPL, these equations have been developed into MAT-LAB programs that can be found in Appendix B.2.1. These programs allow the user to input their propeller parameters and operating conditions such as thrust, torque and forward-speed Mach number. The root-mean-square pressure p'_{rms} is then calculated for the near field using equation (4.6) and for the far field using (4.12).

By default the field points for the near field are scattered on a circle with the radius $2D$ in the x - y plane as seen in figure 4.1(a). This was done using polar coordinates for the field points with the values $x = 2D\cos\phi$, $y = 2D\sin\phi$ and $z = 0$, where ϕ is the polar angle. Because of symmetry around the x-axis it is usually sufficient to look at only half a circle. Figure 4.1(b) instead depicts the default positions for the field points when calculating the far field SPL using equation (4.12). The far field observers were scattered on a line of length $200D$ that is located $100D$ below the propeller.
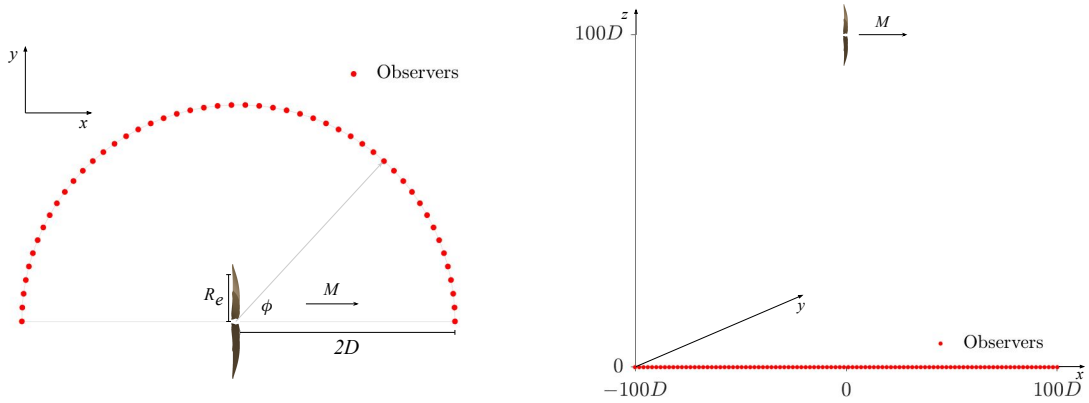
(a) Schematic of 50 observers spread out on a half-circle.

(b) Schematic of 100 observers along the x-axis.

Figure 4.1: Schematic views of the observers in the near and far field, respectively.

For the study of multiple propellers and their distribution, the SPL is calculated for both the near and far field. Time is taken into account, and as such, equation (4.6) and (4.12) can not be used. Instead, equations (4.1) and (4.2) are used for the near field while equation (4.9) and (4.10) are used for the far field. To calculate the pressure from multiple propellers on a single observer, the pressure from each propeller is calculated individually and then added together before the root mean square pressure is calculated.

$$p'_{tot} = \sum_{x=1}^{n} p'_{Tx} + p'_{Qx} \tag{4.13}$$

Here, n refers to the total number of propellers on the plane.

4.2 Verification

To verify the credibility of the MATLAB programs, the near field calculations were compared to examples provided by Garrick and Watkins [6]. The acoustic data was manually extracted from their graphs and the same propeller parameters and operating conditions were used, which can be found in table 4.1. The root-mean-square total pressures p'_{rms} were then calculated along a line 6 feet above the propeller and the predicted data was plotted alongside the reference data for comparison, see figures 4.2 and 4.3. Particular care had to be taken due to the given parameters being provided in imperial units instead of SI units. The conversion from pounds per square foot to dynes per square centimeter was done by multiplying the data with a factor of 480, which is what was used by Garrick and Watkins.

Table 4.1: Parameters from Garrick and Watkins [6] used to verify the programs.

Flight Mach number	0	0.8	-
Thrust	1850	310	lb.
Efficiency	0	62	%
Blade count	2	2	-
Diameter	10	10	ft
Torque	2680	2680	lb-ft
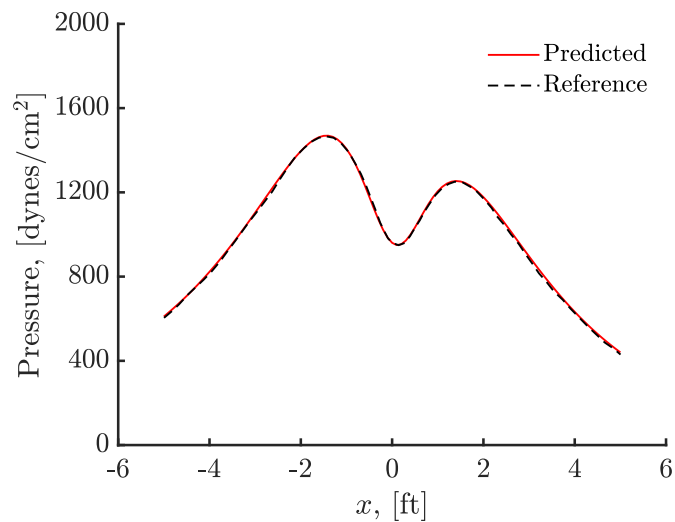
Figure 4.2: Verification of root-mean-square pressure levels at forward-speed Mach number $M = 0$.
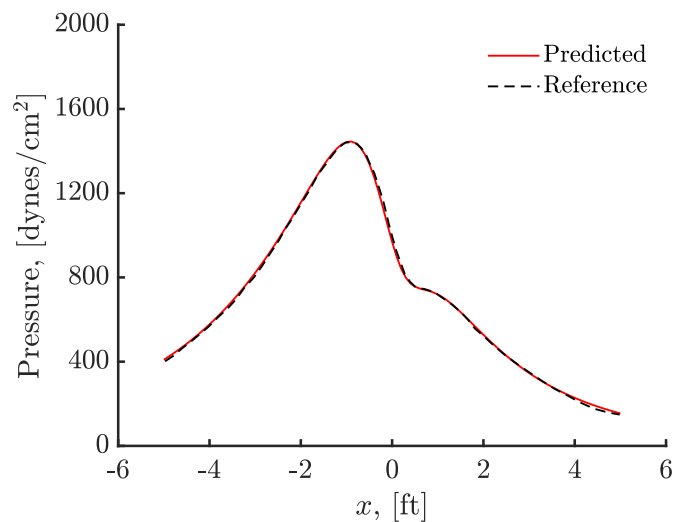
Figure 4.3: Verification of root-mean-square pressure levels at forward-speed Mach number $M = 0.8$.

As can be seen in these figures, data calculated using equation (4.6) is almost identical to the reference data. The few discrepancies can most likely be attributed to errors from digitally extracting the reference data. It was decided to keep the pressure data in units of dynes/cm^2 and feet along the x-axis to stay true to the reference and to avoid introducing unnecessary unit transforms for the verification. Because the MATLAB programs provided data matching that of the reference, it was concluded that they were working as intended and deemed satisfactory.

4.3   Baseline Propeller Noise

The next step was to establish the acoustic data for the baseline propeller model, i.e. a propeller with six blades, a diameter of 2.2 meters and a rotational speed of 2200 revolutions per minute. The full list of operating conditions used for the acoustic calculations of the baseline propeller can be found in table 4.2, notably the efficiency, thrust and torque were calculated through the use of *OptoProp*. The following calculations were all done at a radius of $2D$ from the propeller for the near field and $100D$ below the propeller for the far field.

Table 4.2: Baseline propeller parameters.

Blade count	6	-
Diameter	2.2	m
Rotational speed	2200	RPM
Flight Mach number	0.35	-
Speed of sound	319.9125	m/s
Efficiency	88.0193	%
Thrust	3125.4	N
Torque	1725.619	Nm

As a way to further increase the credibility of the program the near field p'_{rms} was calculated using equation (4.6) and compared to data gathered through the use of more advanced methods, namely Computational Fluid Dynamics (CFD) and the Ffowcs Williams and Hawkings (FW-H) equations (acoustic data can be found in Appendix B.1.1). Both of these calculations used the parameters and operations conditions found in 4.2 and the comparison can be seen in figure 4.4(a). Notably, a dip in the SPL is visible for the observers around the 60° polar angle. This is likely inherent to the formulas used, but even so, when compared to data computed using CFD+FW-H the SPL are very similar. Furthermore, the SPLs were also computed for the far field using both equation (4.6) and (4.12), that is they were both used to calculate the p'_{rms} for the far field observers. Both of these yielded almost the same results which is to be expected as equation (4.6) used for the near field should reduce to equation (4.12) at greater distances. As can be seen in figure 4.4, the far field equation (4.12) displayed a lower SPL at the spot where they both drastically dip; this could be considered a singularity of sorts.
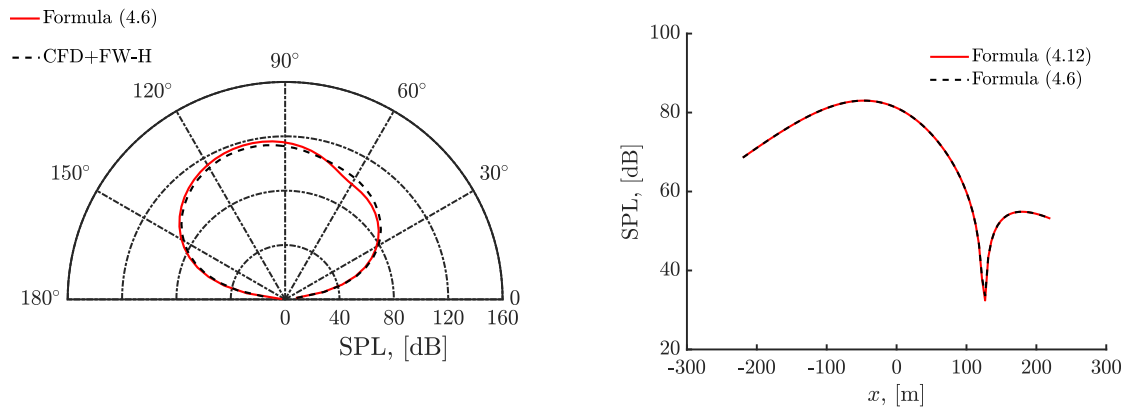
(a) Comparison of the SPL calculated using CFD+FW-H and equation (4.6).

(b) Comparison of the SPL for the far field using both equations (4.12) and (4.6).

Figure 4.4: Baseline propeller noise for the near and far field.

It can also be of considerable interest to view the acoustic data in three dimensions. Because of this, the near field program was expanded to calculate the SPL for field points scattered across the surface of a sphere instead of a circle. The observer coordinates (x,y,z) were given the values $x = 2D\cos\phi\sin\Theta$, $y = 2D\sin\phi\sin\Theta$ and $z = 2D\cos\Theta$, where ϕ is the azimuthal angle and Θ is the inclination. The far field was extended to allow the observers, or field points, to occupy a flat plane with the dimensions $20D$ in width and $200D$ in length which can be seen in figure 4.6. The propeller was still considered to be moving uniformly along the x-axis.
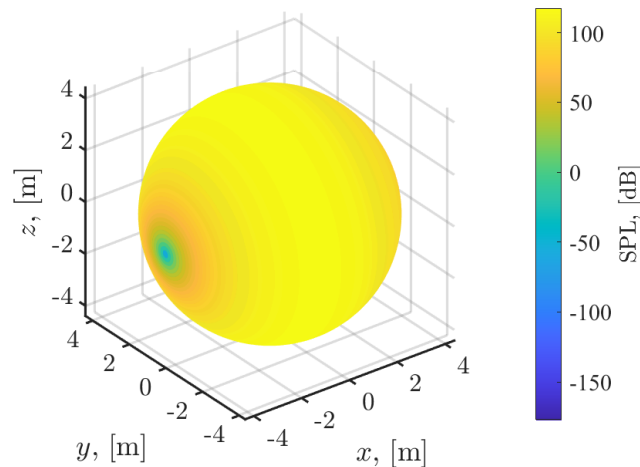
Figure 4.5: Visual representation of the 3D acoustic data of the near field for the baseline propeller.
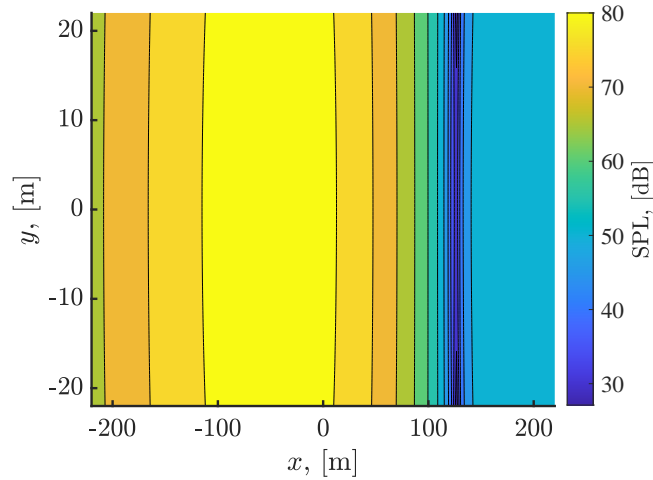
Figure 4.6: Acoustic calculations for a flat plane in the far field for the baseline propeller.

Both of these images clearly show the SPLs displaying symmetry around the x-axis, but also that the areas experiencing the loudest noise levels are located behind this particular propeller. The flat contour of the far field also does not show much curvature but this is likely due to the width of the plane being short in comparison to the altitude. That is to say the distance between the field points and source does not change significantly when the value of y is limited to $\pm 10D$ while $z = 100D$.

4.4 Sound from Propellers with Various Parameters

The programs were then used to study the effects each parameter had on the total p'_{rms}. This was done by following the same methodology as in chapter 3.1, alternating the parameters as in table 3.1. This limited the parameters that were studied to blade count, propeller diameter and rotational speed. Just like previously they were studied by changing one parameter at a time and keeping the others with the values of the baseline propeller model. While studying the effects of each parameter on the SPL, both the near field and far field were calculated like before, i.e. the near field on a circle with a radius of $2D$ around the propeller and the far field along a line with a length of $200D$ located $100D$ below the propeller. The results are visualised in the following figures where the red lines indicate the baseline propeller.

(a) Blade count effects on the near field.

(b) Blade count effects on the far field.
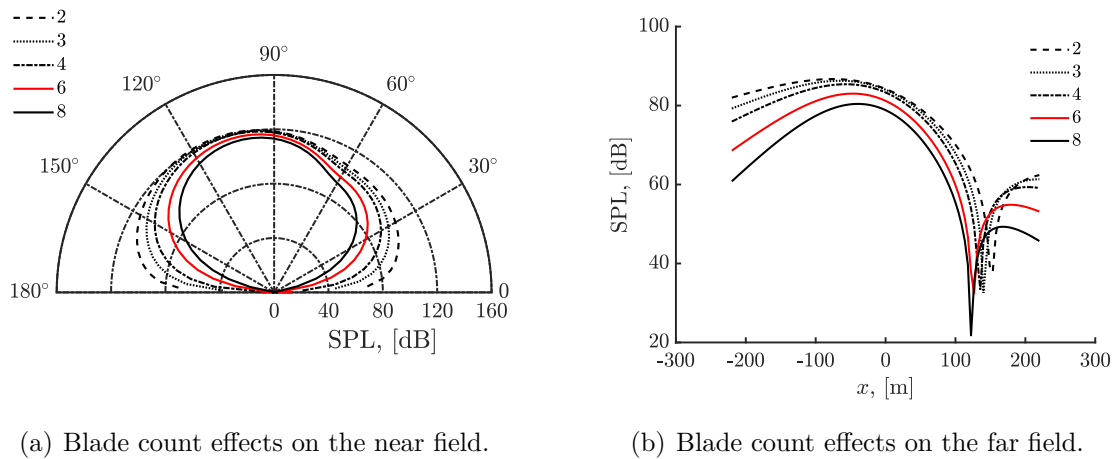
Figure 4.7: Visualisation of how different blade counts affect the SPL.

The varying blade counts show an impact on the SPL for both the near field and the far field. As can be seen in figure 4.7, an increased blade count actually has the effect of decreasing the SPL. In the near field (figure 4.7(a)) this is most noticeable at the polar angles relatively close to the x-axis. However, the peak amplitudes are not affected as much and the general shape is largely the same. The far field (figure 4.7(b)) sees a similar occurrence where the SPL decrease with a rising blade count. With an increased blade count, both the peaks in front of and behind the propeller see a decrease in amplitude and the dip in SPL in front of the propeller moves closer to the source.

(a) Propeller diameter effects on the near field.

(b) Propeller diameter effects on the far field.
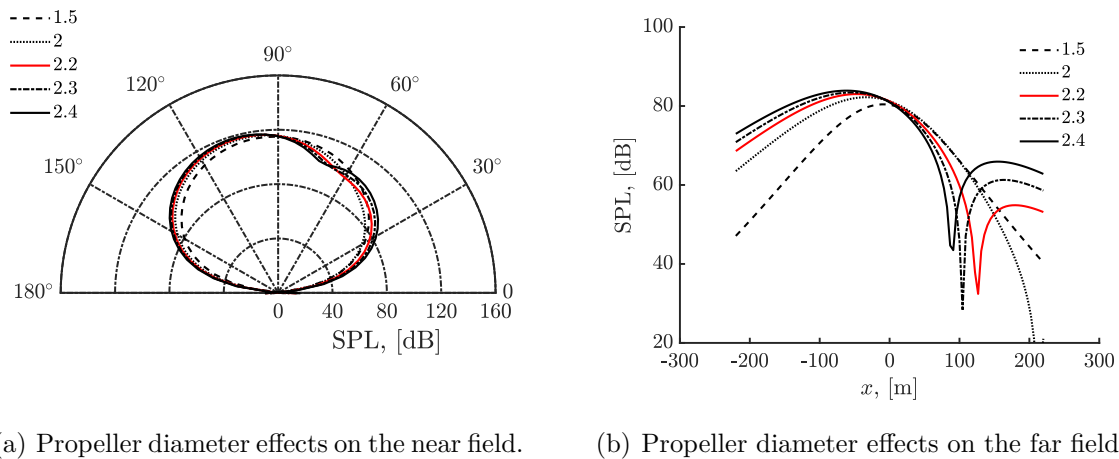
Figure 4.8: The impact propeller diameter has on the SPL.

Varying the propeller diameter instead generates some different results. The different values of D did not show much of an impact on the near field (figure 4.8(a)) but the effects on the far field (figure 4.8(b)) can be of interest instead. It should be noted that because these calculations were done along a line of length $200D$, the baseline diameter was chosen for this purpose to stay consistent with the placement of the observers. When looking at the graph, a reasonable assumption to make is

31

that all of the graphs follow the same shape, i.e. a peak behind (or close to) the propeller followed by a significant drop in front before experiencing another peak further ahead. The graphs seem to indicate that the drop in SPL occurs further ahead of the propeller with a decreasing diameter and the SPL falls of quicker behind the propeller. The peak in front of the propeller also has a noticeable decrease in SPL with a decreasing diameter.
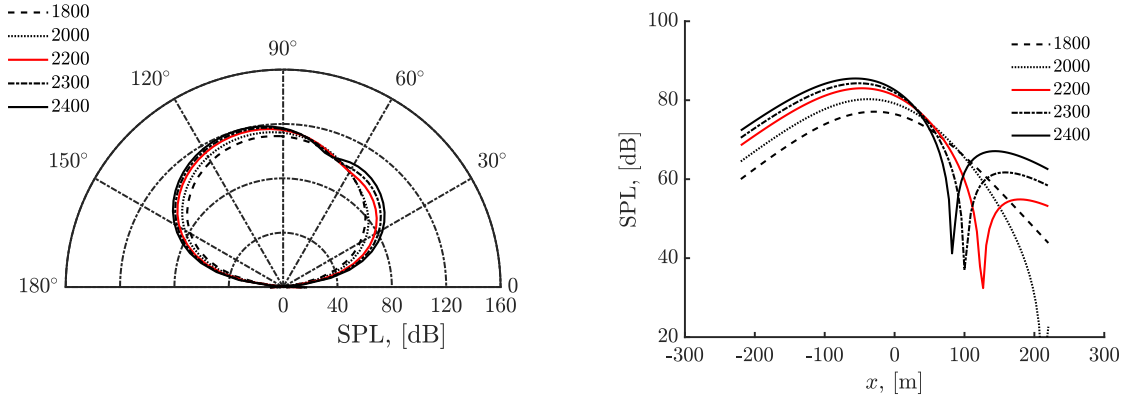
(a) Rotational speed effects on the near field.

(b) Rotational speed effects on the far field.

Figure 4.9: The impact rotational speed has on the SPL.

Altering the rotational speed show very similar results as when altering the propeller diameter. The near field (figure 4.9(a)) retains the same general shape and especially the lower rotational speeds decrease the SPL but the change is almost insignificant. The far field also displays a similar appearance as that of the alternating diameters. The difference is that the peak behind the propeller does not fall off nearly as quickly. Both the drop in SPL and the peak in front of the propeller seems to behave much like the SPL when varying the diameter, however.

The combined impact on SPL of blade count and rotational speed was then studied. This was also done following the same methodology as in the earlier parameter research, with values taken from table 3.1. The SPL were studied for both the near field and far field by choosing a single observer, for the near field that was at the polar angle 90° and for the far field at $x = 0$. The SPL is plotted against the tip Mach number which increases with the rotational speed (see equation (3.2)) and each blade count is displayed as a separate graph, which can be seen below.
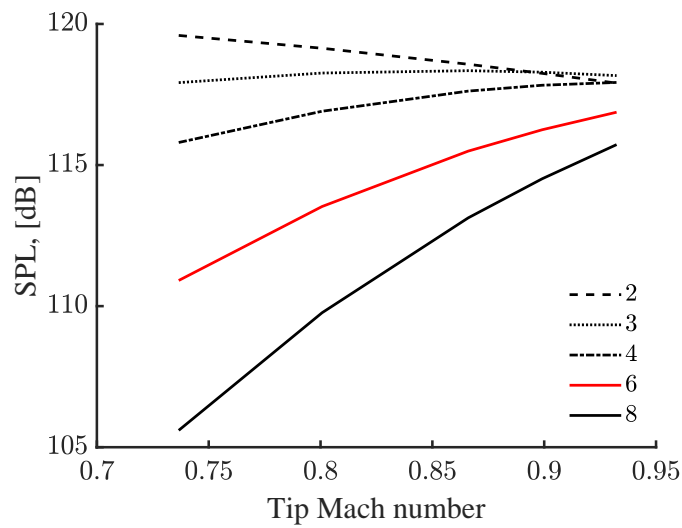
Figure 4.10: The combined effect of blade count and rotational speed on the near field.
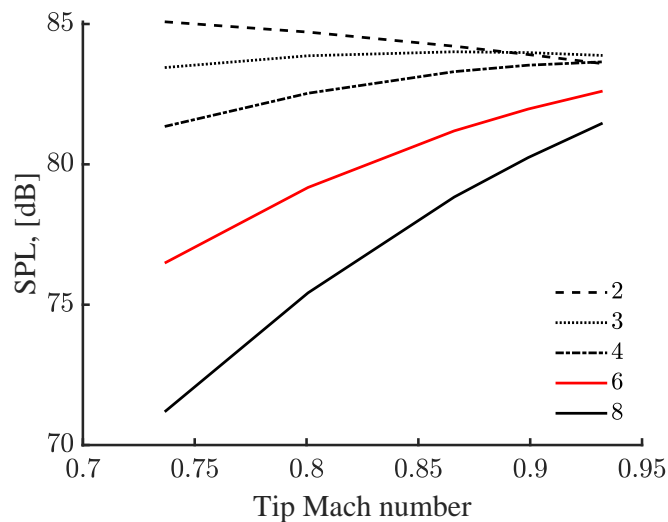
Figure 4.11: The combined effect of blade count and rotational speed on the far field.

These graphs visualise the two factors contributing to the noise levels, those being the aerodynamic forces and the tip Mach number. Both of these graphs looks very similar for the near and far field, only difference being the SPL. The tip Mach number is the more dominant factor which is why increasing the blade count, and thus decreasing the noise, will not have the same effect at every rotational speed. When designing a propeller a balance must be struck where the gain from an increased blade count is not neglected by a high tip Mach number, e.g. eight blades at tip Mach number 0.85 will have roughly the same SPL as six blades at tip Mach number 0.75.

4.5   Sound from Multiple Propellers

Lastly, the SPLs were also studied for configurations with multiple propellers, all with identical properties but with different distributions on the airplane. This means that the total SPLs from different propeller placements can be studied. In the studied propeller distributions there are seven different propeller positions (see figure 3.8(b)) and the coordinates for these positions can be found in table 4.3 below.

Table 4.3: Table containing all used propeller locations for the multiple propeller testing.

Number	1	2	3	4	5	6	7
x	0	0	$-5D$	0	0	0	0
y	0	0	0	0	0	0	0
z	$2D$	$-2D$	0	$-3D$	$3D$	$-4D$	$4D$

Specifically, four different propeller distributions were studied and the propellers used in each distribution can be found in the following table 4.4.

Table 4.4: The propellers used in each distribution.

Distribution number	Propellers
1	1, 2
2	1, 2, 3
3	1, 2, 4, 5
4	1, 2, 4, 5, 6, 7

When running these distributions through a MATLAB program, implementing the method described at the end of chapter 4.1, SPLs are calculated for each distribution in both the near and far field. The observers are placed in a line for both the near and the far field, similar to figure 4.1(b). In the near field, the observers are placed in a $20D$ long line at a distance of $4D$, and in the far field the line is $200D$ long, placed at a distance of $100D$ away from the origin. Calculating the SPL at each observer and then plotting the SPL for each distribution in the same graph resulted in the figures 4.12(a) and 4.12(b). Each individual plot can be found in appendix B.1.2.

(a)

(b)
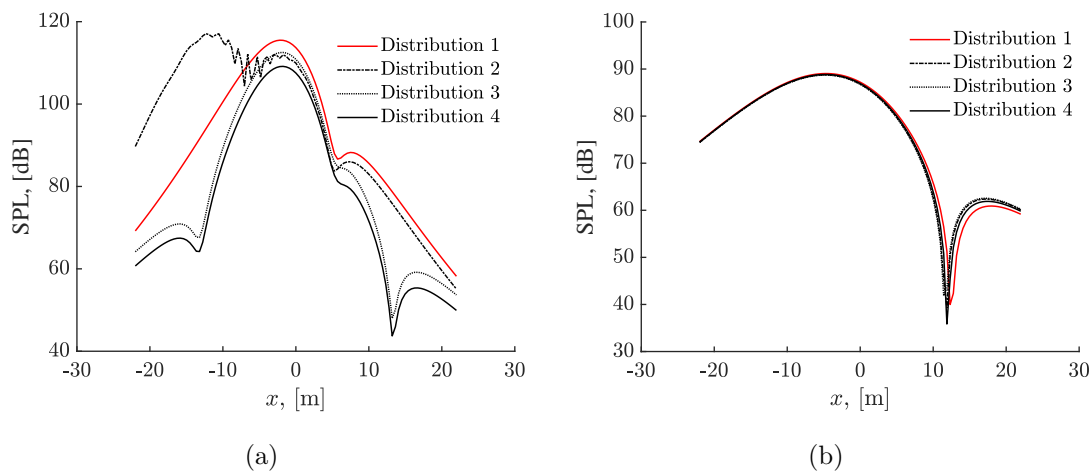
Figure 4.12: The SPL for each distribution in the near field, (a) and far field, (b) respectively.

Lastly, the program was modified to calculate the SPLs for a plane in the fair field, similar to figure 4.6. With the aircraft traveling in the positive direction of the x-axis, figure 4.13 provides a visual representation of what the plane shows, that is how loud the noise is for a plane $100D$ from the aircraft. Since the SPL in the far field is the same for all distributions, only one plane needed to be calculated, where the colour bar shows what magnitude of sound each colour represents.
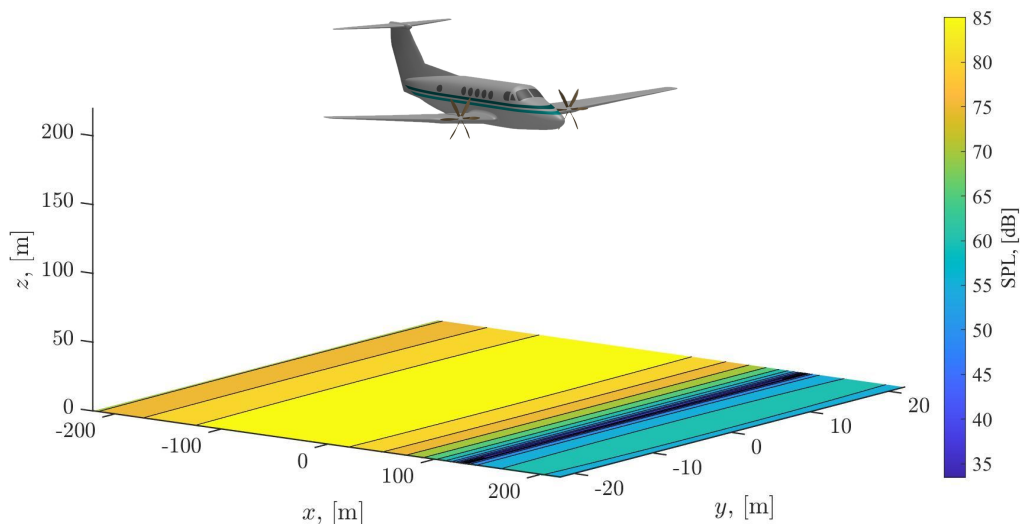
Figure 4.13: Visual representation of an aircraft above the far field plane. Source for aircraft model: [12].

Looking at the overall tendencies of the noise, it is apparent that the SPL in the far field is barely affected by the number of propellers or their placement, while the near field depends on both. In the near field, propeller distribution two, found in table 4.4, has the highest peak, caused by propeller three. Distribution one has the highest overall SPL, while distribution three and four are the lower ones, with distribution four being the most optimal propeller distribution, out of the four, for a low-noise aircraft.

5
Conclusions

5.1 Propeller Design Research

The parameter study has resulted in a clear visual presentation of how different parameters affect the propeller efficiency and the aircraft's ability to generate torque. The general trend of the research shows that individually each parameter at its highest value generates the most efficient propeller. This trend was repeated for multiple propellers where the higher values resulted in a high efficiency. What can be seen though, is that at the maximum blade count together with a high tip Mach number the trend of an increased efficiency changes and the line in figure 3.7 slightly falls. This would imply that simply increasing all separate parameters does not result in the most highly effective aircraft propeller. It was also noted that altering the propeller diameter significantly changes the propeller efficiency compared to the other parameters. Usage of a small diameter would therefore, according to this research generate a highly inefficient propeller.

Based on this study the conclusion is therefore that if possible a high number of blades is the most optimal choice for an electric aircraft. Although it needs to be controlled that the angular velocities are not too high or this will lead to reversible effects resulting in the propeller being less efficient.

The research on multiple propellers illustrates that increasing the propeller count increases the individual propeller efficiency. This trend continues up to four propellers at which the trend changes and the efficiency starts to decrease. What can be noted is that the efficiency increase from two to four is greater than the decrease from four to six. This implies that six propellers are more efficient than using two as seen in table 3.2.

5.2 Propeller Noise Simulations

The acoustic study has made a distinction between the sound generated close to the propeller and that generated relatively far away, the same distinction should also be made when looking at the impact of each parameter. However, in general it can be said that for a single propeller an increased blade count should result in lower noise levels while increasing the diameter and rotational speed will increase the noise. This is likely because they both affect the tip Mach number which at higher values seems to be the dominant factor affecting the SPLs.

If the aim of designing a single propeller is to decrease the SPLs experienced for example in the cabin, the parameter of interest should be the blade count. Increasing this had a substantial effect on the noise levels, especially in the areas right behind or right in front of the propeller. The propeller diameter and rotation speed did not show much of an impact unless going for the lower-end values, although these parameters should not be of major interest when purely trying to decrease SPLs in the near field.

Decreasing the noise from a single propeller in the far field is not as clear, however. While increasing the blade count and decreasing the diameter and rotational speed also tends to decrease the SPL, the location of the peaks should also be taken into consideration. One could argue that the distance between the peaks and dips in relation to the propeller does not matter as much, because if the airplane is traveling forward the observers will experience the same peaks either way. Rather, a quick fall-off could be desirable, meaning that a smaller area experiencing the noise at every given moment should be desired. If looking at the big peak behind the propeller for example, both the blade count and diameter seem to fall off quicker than the rotation speed which appears to fall off almost linearly. If the choice is to decrease either the diameter or rotation speed, the diameter could be considered preferable when looking at the shape of the curves.

When increasing the number of propellers, there is no significant difference in the SPL for the far field, which is clear when looking at figure 4.12(b). Propeller placement also seems to have no large impact on the noise levels since distribution two, with propeller three, which is places further back on the plane compared to the other propellers, has the same SPL as the other three distributions.

In the near field there is a more clear difference between the different distributions, which can be seen in figure 4.12(a). Distribution two is the odd one out here, with another peak caused by propeller three. It is also the distribution with the highest peak SPL while distribution one has the highest overall after this peak. Distribution three and four clearly has a lower SPL than the other two, with distribution four having the lowest. This means that, out of the calculated propeller distributions, distribution four is the most suitable when designing a low-noise aircraft.

5.3 Guidelines for Low-Noise Propeller Design

Examining the individual parameters effect on the propeller efficiency, and comparing those with the results from the acoustic studies, it was established that separate parameters have conflicting effects within the two studies. The purpose of this section is therefore to discuss an optimal way to improve the noise emissions without having an significant impact on the overall efficiency.

Benefiting from using a small diameter resulting in less noise radiation in the far field the design concluded that the efficiency falls when the diameter is decreased.

The result from this comparison is that the choice of diameter should be based on reaching a sought-after noise radiation while avoiding the use of too small of a propeller hurting its efficiency. If a low noise level in the near field is desired, the diameter will have negligible impact and the diameter should be chosen for the maximum efficiency.

Similarly, the rotational speed can also be increased to achieve a more efficient propeller based on the design study. However, this will have a negative impact on the noise, more so the far field rather than the near field which is nearly inconsequential. When varying the rotational speed both the efficiency and SPLs at the far field behave much like when changing the diameter. However, the rotational speed was also studied on conjunction with the blade count and this time both studies also showed similar trends. The gains from increasing the blade count were not as substantial at higher rotational speed compared to the lower ones.

As mentioned previously, both studies indicated that increasing the number of blades results in a positive impact on both efficiency and noise levels. The studies were performed with blade counts varying from two to eight blades where every increase resulted in an increasing efficiency and simultaneously a decrease in the noise levels for both the near and far field. It should be noted that the gain in efficiency was most noticeable when increasing an already low blade count, e.g. two to three blades compared to six to eight. This effect was not as prominent when looking at the noise levels and it is still indicative of a higher blade count being beneficial.

Based on the analysed results considering both individual studies, final decisions can be made in order to create an highly efficient yet low noise propeller. Considering the key factors mentioned under this section a recommended propeller layout would be a four propeller setup, attempting to maximise the amount of blades for each individual propeller. The diameter should be relatively small for low noise radiation but the efficiency has to be considered which would result in a diameter around 2 m, the angular velocity can be fairly high although around 2300 with a high blade count the efficiency is decreased according to the design research.

When comparing both studies on multiple propellers it is apparent that there are some differences. The propeller efficiency increases with the number of propellers and peaks at four. The decrease after the peak is smaller than the increase before the peak, and as such, it is more efficient to have six propellers compared to two. In the acoustic studies, the far field noise is basically the same for all four distributions and therefore, the chosen distribution has no notable impact on the SPL in the far field. In the near field, there is a clear difference between each propeller distribution, with distribution four being the best alternative to minimise the noise. A trend that is apparent in figure 4.12(a) is that an increasing amount of propellers reduce the near field SPL when placed in a row, while distribution two results in an extra peak. As such, it would then be reasonable to choose between distribution three and four in this case. Distribution three provides a high efficiency with a slightly louder noise, while distribution four is the most silent but with a slightly lower efficiency.

5. Conclusions

6
Ethical Aspects

An ethical analysis was conducted based on the methodology and result of the project. Discussing the moral reasoning behind the choices based on a scientific background.

6.1   Scientific Reasoning Behind the Project

The project has its core focus in advancing the technology and components used in an electric aircraft with the goal to increase efficiency while minimizing noise radiation, in the near field and far field. Designing a propeller with a low impact on the surrounding area and its people is a key factor in the purpose of the project.

There has been studies showing the effect noise produced by traffic and aviation has on the general population, an example of this is the study named NORAH [5]. During five years a number of studies were made to analyse how noise-related annoyance creates health problems in the long term for affected people. The key factors that is pointed out is that people being in areas containing aircraft noise have been found to have an increased chance of depression. There is also a connection between the annoyance from noise and children's ability to learn due to the noise disturbing schools. The main point is that this study shows that people are affected by surrounding noise radiated from airplanes. Therefore, there needs to be improvements made in the area of noise pollution to allow people to live as they please without experiencing any discomfort caused by their surroundings.

6.2   Ethical Analysis

The methodology of the project is constricted to using an in house software rather than using real life testing in a lab environment. This choice of structure allows the project to be conducted without exploiting any natural resources nor affecting people and animals outside of the work group. This ensures that the method does not conflict with individual peoples ethical values allowing them to fully express autonomy outside of the project. What autonomy indicates in this case is that they are not affected in any way by the choices made within the work group from a methodological point of view.

The result from this project is the guidelines for future aviation companies to develop a low-noise propeller while maintaining a high efficiency. Companies will be able

use these guidelines in order to adapt to future regulations and therefore, improving upon existing propellers leading to conventional aircraft generating less noise. Taking the study mentioned in section 6.1 into account, it could then be argued that the result is morally good. It is hard to currently predict the evolution of the aviation industry and its availability of electric airplanes globally although, if the use of these airplanes would increase, the result from this study would benefit the people affected by the generated noise.

The project can not influence the effects leading to increased availability however, the positive impact that the result leads to outweigh the negative factors which indicates that this project was ethically correct to conduct.

7

Future Work

This section gives some thought to what could be further explored in future work. This project is only focused on conventional propellers and it would be interesting compare their performance against different types of propellers such as dual propellers, tandem propellers and ducted propellers. For future work the theory required to design and evaluate these propeller types could be implemented into matlab and the acoustic program.

7.1 Ducted Propellers

Adding a shroud around the propeller, as shown in figure 7.1, shows promising results in reducing the amount of noise emitted from the propeller. It is especially effective in reducing the higher sound harmonics generated from propellers but also the sound pressure and lower frequencies are reduced. The reason for less noise being emitted using a shrouded propeller is because the propeller generates large part of the thrust through suction at the leading edge of the shroud. However, the efficiency is affected by the shape of the shroud and a bad design can lead to increased noise over a conventional propeller [10].

Figure 7.1: Ducted propeller.

7.2 Dual Propellers

The dual propeller also called counter rotating propeller is when two separate propellers placed right behind each other are rotated around the same axis and by the same engine but in opposite directions. The dual propeller can help increase propeller efficiency due to the way air is pushed and flows passed the propeller. By

adding the second propeller the maximum trust can be increased with changing the diameter of the propeller [4]. Regarding the noise emissions for a dual propeller they are similar to that of a single propeller. The noise emissions can be found by adding the noise fields from each individual propeller with respect to the position of the observer. This results in the propeller noise when the two propellers cross being the same as for a single propeller with the same number of blades as one of the two propellers. When the propellers are positioned between the crossing the sound is the same as for a single propeller with same number of blades as the two propellers together [10].
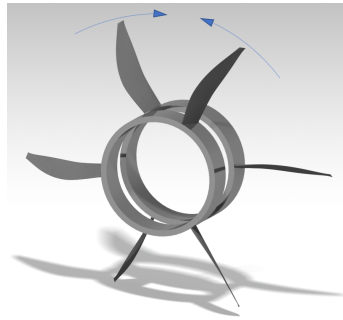
Figure 7.2: Dual propeller setup.

7.3 Tandem Propellers

Tandem propellers are similar to dual propellers but two propellers are rotating in the same direction instead of the opposite. This type of propeller is suitable for applications that require a lot of power. If the two propellers have same amount of blades and equal spacing between the noise is almost the same as for a single propeller with the same blade count. Certain frequencies of the sound can be cancelled out by having different spacing between the blades, however not without increasing other frequencies [10].
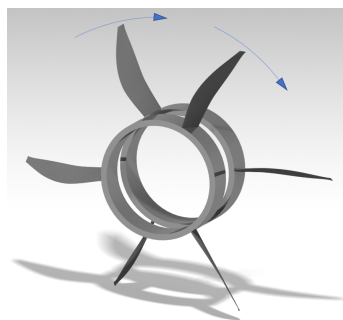
Figure 7.3: Tandem propeller.

Bibliography

[1] International Air Transport Association, "Fact Sheet Climate Change & CORSIA", 2018. [PDF]. Available: `https://www.iata.org/contentassets/c4f9f0450212472b96dac114a06cc4fa/\fact-sheet-climate-change.pdf/`, accessed: 2020-05-04

[2] Air Transport Action Group. "Facts & Figures", 2020. [Online]. Available: `https://www.atag.org/facts-figures.html`, accessed: 2020-05-04

[3] International Air Transport Association "IATA Forecast Predicts 8.2 billion Air Travelers in 2037", 2018. [Online] Available: `https://www.iata.org/en/pressroom/pr/2018-10-24-02/`, accessed: 2020-05-04

[4] SKYbrary, "Contra-Rotating Propeller", 2017. [Online]. Available: `https://www.skybrary.aero/index.php/Contra-Rotating_Propeller`, accessed: 2020-05-11

[5] Gemeinnützige Umwelthaus GmbH, "NORAH Noise Impact Study." 2015. [PDF]. Available: `http://www.laermstudie.de/fileadmin/norah/NORAH_Wissen/\EN/NORAH_Knowledge_14.pdf`, accessed: 2020-02-28

[6] I. E. Garrick and C. E. Watkins. "A Theoretical Study of the Effect of Forward Speed on the Free-Space Sound-Pressure Field Around Propellers.".Tech. rep., NACA, Oct 1953. [PDF]. Available: `https://ntrs.nasa.gov/archive/nasa/casi.ntrs.nasa.gov/19930092212.pdf`, accessed: 2020-02-04

[7] C. N. Adkins and R. H. Liebeck "Design of Optimum Propellers", *Journal Of Propulsion And Power*, Vol. 10, No.5, 1994. [PDF] accessed: 2020-02-04

[8] A. Capitao Patrao, "Implementation of Blade Element Momentum/Vortex Methods for the Design of Aero Engine Propellers", Research Report, Department of Mechanics and Maritime Sciences, Chalmers University of Technology, 2017. [PDF]. Available: `https://research.chalmers.se/publication/253423`, accessed: 2020-02-04

[9] Z. J. Huang and H. D. Yao, "Propeller Design for Quiet Electric Aircraft". [PDF].

[10] A. A. Regier and H. H. Hubbard, "Status of research on propeller noise and its reduction", *The Journal of the Acoustical Society of America,* 1953. [PDF]. Available: `https://asa.scitation.org/doi/10.1121/1.1907054`, accessed: 2020-02-04

[11] J. Roskam and C. T. Lan "Airplane Aerodynamics and Performance", Design, Analysis and Research Corporation. 1997, accessed: 2020-04-21

[12] S. Ozmumcu "Beechcraft King Air B-200," 3D model, 2011. [Online]. Available: `https://grabcad.com/library/beechcraft-king-air-b-200--1`, accessed: 2020-04-27

[13] D. Frisk, "A Chalmers University of Technology Master's thesis template for LATEX," 2018. [Online]. Available: `https://sv.overleaf.com/latex/templates/chalmers-university-of-technology-masters-thesis/vjstprwccbqc`

A

Appendix A

A.1 Data Used for Single Parameter Study

This section includes the data used for the graphs created in during the design of the propeller. The data is visualised as tables for each of the studies.

A.1.1 Alternation of Blade Count

Table A.1: Data calculated for alternation of blade count as a single parameter.

Blade count	2	3	4	6	8	-
Coefficient of thrust	0.137	0.137	0.137	0.137	0.137	-
Efficiency	81.2	83.6	85.4	88.0	88.7	%
Torque	1870.64	1817.4	1779.3	1725.74	1712.96	Nm

Table A.2: Table with all lift coefficients for the graph with alternating blade numbers, each lift in a column is for a separate section of the airfoil.

Blade count	2	3	4	6	8
Coefficient of lift					
	1,106	0,685	0,483	0,293	0,209
	1,232	0,765	0,540	0,329	0,234
	1,329	0,827	0,584	0,356	0,254
	1,394	0,870	0,616	0,376	0,268
	1,440	0,901	0,639	0,391	0,278
	1,471	0,923	0,656	0,402	0,287
	1,494	0,940	0,670	0,412	0,294
	1,508	0,952	0,680	0,419	0,299
	1,514	0,959	0,686	0,425	0,304
	1,512	0,961	0,690	0,428	0,307
	1,504	0,959	0,690	0,430	0,309
	1,491	0,953	0,688	0,431	0,310
	1,475	0,946	0,685	0,431	0,310
	1,457	0,938	0,682	0,430	0,311
	1,441	0,930	0,678	0,430	0,312
	1,424	0,923	0,675	0,430	0,313
	1,408	0,915	0,671	0,430	0,314
	1,393	0,909	0,669	0,431	0,315
	1,380	0,903	0,667	0,432	0,317
	1,367	0,898	0,665	0,433	0,319
	1,355	0,892	0,663	0,434	0,321
	1,347	0,890	0,663	0,436	0,324
	1,342	0,890	0,665	0,440	0,329
	1,338	0,889	0,667	0,443	0,333
	1,334	0,889	0,669	0,447	0,337
	1,334	0,892	0,673	0,452	0,342
	1,337	0,896	0,678	0,458	0,349
	1,340	0,900	0,683	0,464	0,354
	1,345	0,906	0,689	0,470	0,361
	1,349	0,911	0,694	0,476	0,367
	1,354	0,916	0,700	0,483	0,374
	1,360	0,922	0,706	0,489	0,381
	1,368	0,930	0,714	0,497	0,388
	1,375	0,936	0,720	0,503	0,395
	1,378	0,940	0,724	0,508	0,400
	1,377	0,941	0,726	0,512	0,405
	1,372	0,939	0,726	0,513	0,407
	1,365	0,936	0,724	0,514	0,409
	1,350	0,927	0,719	0,511	0,409
	1,328	0,913	0,709	0,506	0,405
	1,294	0,891	0,693	0,495	0,398
	1,250	0,862	0,671	0,481	0,387
	1,197	0,826	0,643	0,462	0,373
	1,131	0,781	0,609	0,439	0,355
	1,051	0,726	0,567	0,409	0,331
	0,955	0,660	0,516	0,373	0,303
	0,844	0,584	0,456	0,330	0,268
	0,718	0,497	0,389	0,282	0,229
	0,578	0,400	0,313	0,227	0,185
	0,426	0,295	0,231	0,168	0,137

A.1.2 Alternation of Diameter

Table A.3: Data calculated for alternation of diameter as a single parameter.

Diameter	1.5	2	2.2	2.3	2.4	m
Coefficient of thrust	0.634	0.200	0.137	0.115	0.097	-
Efficiency	62.7	84.1	88.0	89.2	89.5	%
Torque	2423.81	1805.65	1725.62	1702.82	1697.33	Nm

Table A.4: Table with all lift coefficients for the graph with alternating diameter, each lift in a column is for a separate section of the airfoil.

Blade count	2	3	4	6	8
Coefficient of lift					
	0,858	0,375	0,293	0,262	0,236
	1,005	0,425	0,329	0,292	0,261
	1,142	0,466	0,356	0,315	0,280
	1,262	0,498	0,376	0,330	0,292
	1,372	0,524	0,391	0,342	0,301
	1,475	0,545	0,402	0,350	0,306
	1,573	0,564	0,412	0,356	0,311
	1,665	0,579	0,419	0,361	0,314
	1,750	0,592	0,425	0,364	0,315
	1,827	0,602	0,428	0,366	0,316
	1,895	0,609	0,430	0,367	0,315
	1,956	0,614	0,431	0,366	0,314
	2,010	0,617	0,431	0,365	0,312
	2,061	0,620	0,430	0,364	0,311
	2,110	0,623	0,430	0,363	0,309
	2,156	0,625	0,430	0,362	0,308
	2,200	0,628	0,430	0,362	0,307
	2,243	0,631	0,431	0,362	0,307
	2,286	0,634	0,432	0,362	0,307
	2,326	0,637	0,433	0,362	0,307
	2,365	0,641	0,434	0,363	0,307
	2,408	0,646	0,436	0,365	0,308
	2,456	0,652	0,440	0,368	0,310
	2,501	0,659	0,443	0,370	0,312
	2,546	0,665	0,447	0,373	0,315
	2,597	0,673	0,452	0,377	0,318
	2,651	0,683	0,458	0,382	0,322
	2,703	0,692	0,464	0,387	0,326
	2,758	0,702	0,470	0,392	0,330
	2,810	0,712	0,476	0,397	0,335
	2,862	0,721	0,483	0,402	0,339
	2,914	0,731	0,489	0,408	0,344
	2,971	0,743	0,497	0,414	0,349
	3,021	0,752	0,503	0,419	0,353
	3,062	0,760	0,508	0,423	0,357
	3,093	0,766	0,512	0,426	0,359
	3,112	0,768	0,513	0,428	0,360
	3,123	0,769	0,514	0,428	0,361
	3,116	0,766	0,511	0,426	0,359
	3,088	0,757	0,506	0,421	0,355
	3,031	0,742	0,495	0,413	0,348
	2,947	0,720	0,481	0,401	0,338
	2,838	0,692	0,462	0,385	0,325
	2,696	0,657	0,438	0,365	0,308
	2,517	0,612	0,409	0,341	0,287
	2,297	0,558	0,373	0,311	0,262
	2,037	0,495	0,330	0,275	0,232
	1,738	0,422	0,282	0,235	0,198
	1,402	0,340	0,227	0,189	0,160
	1,035	0,251	0,168	0,140	0,118

A.1.3 Alternation of Angular Speed

Table A.5: Data calculated for alternation of rotational velocity as a single parameter.

Angular speed	1800	2000	2200	2300	2400	RPM
Coefficient of thrust	0.205	0.166	0.137	0.125	0.115	-
Efficiency	84.7	86.6	88.0	88.4	88.6	%
Torque	2191.19	1928.74	1725.62	1642.87	1571.81	Nm

Table A.6: Table with all lift coefficients for the graph with alternating angular speeds, each lift in a column is for a separate section of the airfoil.

Blade count	2	3	4	6	8
Coefficient of lift					
	0,330	0,310	0,293	0,286	0,280
	0,378	0,351	0,329	0,319	0,310
	0,418	0,385	0,356	0,344	0,332
	0,451	0,410	0,376	0,361	0,347
	0,479	0,431	0,391	0,373	0,357
	0,502	0,448	0,402	0,382	0,364
	0,524	0,462	0,412	0,390	0,370
	0,542	0,475	0,419	0,395	0,374
	0,558	0,484	0,425	0,399	0,376
	0,571	0,492	0,428	0,401	0,376
	0,582	0,497	0,430	0,402	0,376
	0,590	0,501	0,431	0,401	0,375
	0,596	0,503	0,431	0,400	0,373
	0,602	0,506	0,430	0,399	0,371
	0,607	0,507	0,430	0,398	0,369
	0,613	0,510	0,430	0,397	0,368
	0,617	0,511	0,430	0,397	0,367
	0,622	0,514	0,431	0,397	0,367
	0,628	0,516	0,432	0,397	0,366
	0,633	0,519	0,433	0,397	0,367
	0,638	0,521	0,434	0,398	0,367
	0,644	0,525	0,436	0,400	0,369
	0,652	0,531	0,440	0,403	0,371
	0,659	0,535	0,443	0,406	0,374
	0,667	0,541	0,447	0,410	0,377
	0,677	0,547	0,452	0,414	0,381
	0,687	0,555	0,458	0,419	0,385
	0,697	0,562	0,464	0,424	0,390
	0,708	0,571	0,470	0,430	0,395
	0,718	0,578	0,476	0,436	0,400
	0,729	0,586	0,483	0,441	0,405
	0,739	0,594	0,489	0,447	0,411
	0,751	0,604	0,497	0,454	0,417
	0,762	0,612	0,503	0,460	0,422
	0,770	0,618	0,508	0,464	0,427
	0,776	0,622	0,512	0,468	0,430
	0,779	0,624	0,513	0,469	0,431
	0,780	0,625	0,514	0,470	0,431
	0,777	0,622	0,511	0,468	0,430
	0,768	0,615	0,506	0,462	0,425
	0,753	0,603	0,495	0,453	0,416
	0,731	0,585	0,481	0,440	0,404
	0,703	0,563	0,462	0,423	0,388
	0,667	0,534	0,438	0,401	0,369
	0,622	0,498	0,409	0,374	0,344
	0,567	0,454	0,373	0,341	0,313
	0,503	0,402	0,330	0,302	0,278
	0,428	0,343	0,282	0,257	0,237
	0,346	0,276	0,227	0,208	0,191
	0,255	0,204	0,168	0,153	0,141

A.2 Data Used for Multiple Parameter Study

This section includes the data used and calculated in the multiple parameter research found under section 3.2, calculating different helical tip Mach numbers for each number of blades.

Table A.7: Data for different rotational velocities, blade count is equal to 2.

Angular speed	1800	2000	2200	2300	2400	RPM
Coefficient of thrust	0.205	0.166	0.137	0.125	0.115	-
Efficiency	77.0	79.6	81.2	81.5	81.6	%
Torque	2410.96	2098.18	1870.51	1781.58	1706.23	Nm
Tip Mach number	0.74	0.80	0.87	0.90	0.93	-

Table A.8: Data for different rotational velocities, blade count is equal to 3.

Angular speed	1800	2000	2200	2300	2400	RPM
Coefficient of thrust	0.205	0.166	0.137	0.125	0.115	-
Efficiency	79.8	82.1	83.6	83.9	84.1	%
Torque	2325.46	2033.87	1817.27	1730.54	1655.21	Nm
Tip Mach number	0.74	0.80	0.87	0.90	0.93	-

Table A.9: Data for different rotational velocities, blade count is equal to 4.

Angular speed	1800	2000	2200	2300	2400	RPM
Coefficient of thrust	0.205	0.166	0.137	0.125	0.115	-
Efficiency	81.2	83.9	85.4	85.8	86.1	%
Torque	2268.77	1989.77	1779.19	1693.12	1616.99	Nm
Tip Mach number	0.74	0.80	0.87	0.90	0.93	-

Table A.10: Data for different rotational velocities, blade count is equal to 6.

Angular speed	1800	2000	2200	2300	2400	RPM
Coefficient of thrust	0.205	0.166	0.137	0.125	0.115	-
Efficiency	84.7	86.6	88.0	88.4	88.6	%
Torque	2191.19	1928.75	1725.62	1642.87	1571.81	Nm
Tip Mach number	0.74	0.80	0.87	0.90	0.93	-

Table A.11: Data for different rotational velocities, blade count is equal to 8.

Angular speed	1800	2000	2200	2300	2400	RPM
Coefficient of thrust	0.205	0.166	0.137	0.125	0.115	-
Efficiency	84.7	86.6	88.0	88.4	88.6	%
Torque	2191.19	1928.75	1725.62	1642.87	1571.81	Nm
Tip Mach number	0.74	0.80	0.87	0.90	0.93	-

A. Appendix A

VI

B

Appendix B

This section includes the data and MATLAB codes used for calculations in the acoustic studies.

B.1 Data and Graphs

This subsection contains different data points and graphs from the acoustic studies.

B.1.1 Acoustic Data from CFD+FW-H

Polar Angle, Radians	SPL, dB
0,1256637	8,422101
0,1884956	29,29372
0,2513274	43,92092
0,3141593	55,0761
0,3769911	63,99216
0,439823	71,32462
0,5026548	77,46245
0,5654867	82,65432
0,6283185	87,06778
0,6911504	90,82039
0,7539822	93,99747
0,8168141	96,66359
0,8796459	98,87098
0,9424778	100,6676
1,00531	102,1068
1,068142	103,2602
1,130973	104,2327
1,193805	105,1667
1,256637	106,2107
1,319469	107,4465
1,382301	108,8368
1,445133	110,2613
1,507964	111,5931
1,570796	112,7419
1,633628	113,6559
1,69646	114,3087
1,759292	114,6878
1,822124	114,7869
1,884956	114,6014
1,947787	114,1259
2,010619	113,3532
2,073451	112,2735
2,136283	110,8731
2,199115	109,1343
2,261947	107,034
2,324779	104,5427
2,38761	101,6219
2,450442	98,22186
2,513274	94,27713
2,576106	89,69999
2,638938	84,37006
2,70177	78,11701
2,764602	70,68964
2,827433	61,6968
2,890265	50,48117
2,953097	35,8084
3,015929	14,90499

Table B.1: Baseline acoustic data gathered through the use of CFD+FW-H.

B.1.2 Plots from Multiple Propeller Calculations
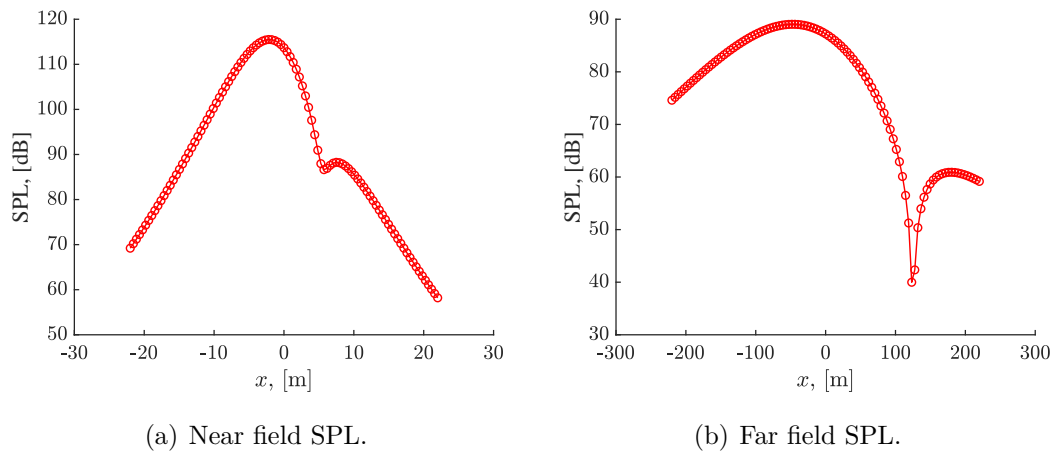

(a) Near field SPL.

(b) Far field SPL.

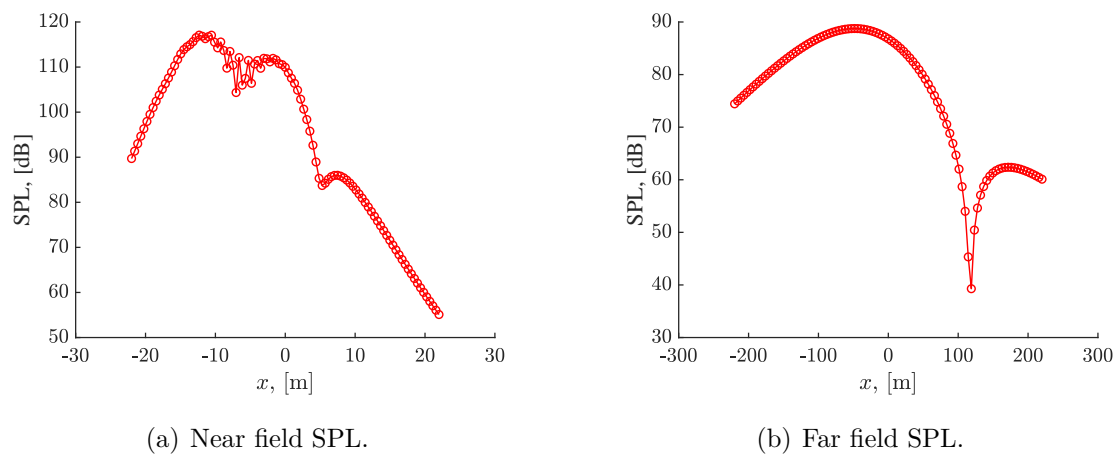**Figure B.1:** SPL of two propellers, distribution 1.
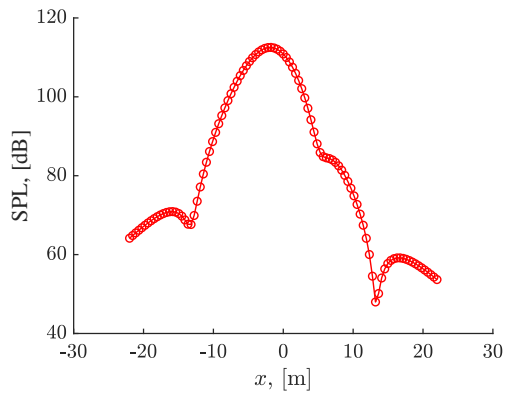

(a) Near field SPL.
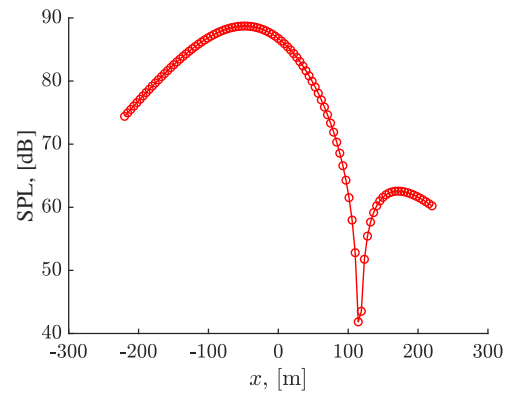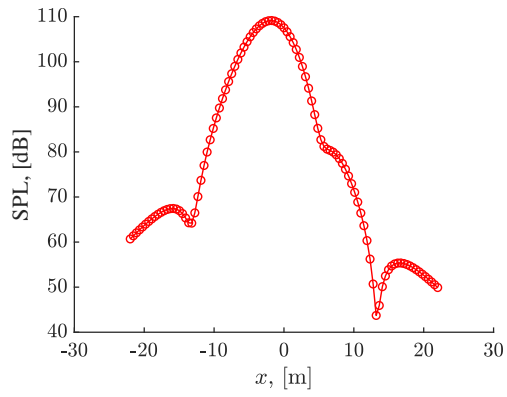
(b) Far field SPL.

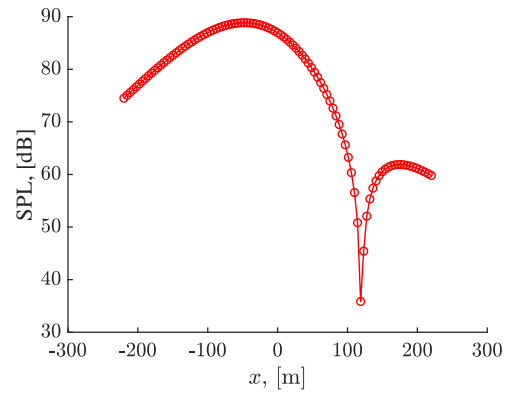**Figure B.2:** SPL of three propellers, distribution 2.

(a) Near field SPL.

(b) Far field SPL.

Figure B.3: SPL of four propellers, distribution 3.

(a) Near field SPL.

(b) Far field SPL.

Figure B.4: SPL of five propellers, distribution 4.

B.2 MATLAB Codes for Acoustic Calculations

The .m-files used for the acoustic calculations can be found below.

B.2.1 Single Propeller

```matlab
function [prmsNearField, SPLNearField] = prmsNearField(m, B, D, M, T, Q, rpm, c0,↩
    Phi)
% Created for MATLAB 2020a or later

    syms theta % Variable of integration
    omega = 2 * pi * rpm / 60; % Angular speed
    k = m * B * omega / c0; % Wave number
    beta = sqrt(1 - M^2);
    R_e = 0.8 * (D / 2); % Effective radius

    % Predefined to reduce runtime
    prmsNearField = zeros(1, length(Phi));
    SPLNearField = zeros(1, length(Phi));
    pref = 2e-5; % Reference pressure 20*10^(-6) Pa

    % Loading coordinates
    x_l = @(theta) 0;
    y_l = @(theta) R_e * cos(theta);
    z_l = @(theta) R_e * sin(theta);

    % Input vector Phi should include the polar angle of every observer
    for i = 1 : length(Phi)

        % Field points, default radius 2D
        x = 2 * D * cos(Phi(i));
        y = 2 * D * sin(Phi(i));
        z = 0;

        S = @(theta) sqrt((x - x_l(theta)).^2 + beta^2 * ((y - y_l(theta)).^2 + (↩
            z - z_l(theta)).^2));
        sigma = @(theta) (M * (x - x_l(theta)) + S(theta)) / beta^2;

        % Functions to integrate
        funA = @(theta) (T .* x ./ S(theta).^2 .* cos(m * B .* theta + k .* sigma↩
            (theta))...
            + (T * k / beta^2 * (M + x ./ S(theta)) - Q * m * B / R_e^2)...
            .* sin(m * B .* theta + k .* sigma(theta))) ./ S(theta);
        funB = @(theta) (-T .* x ./ S(theta).^2 .* sin(m * B .* theta + k .* ↩
            sigma(theta))...
            + (T * k / beta^2 * (M + x ./ S(theta)) - Q * m * B / R_e^2)...
            .* cos(m * B .* theta + k .* sigma(theta))) ./ S(theta);

        % Integrals
        intA = integral(funA, 0, 2 * pi, 'RelTol', 1e-6, 'AbsTol', 1e-6);
        intB = integral(funB, 0, 2 * pi, 'RelTol', 1e-6, 'AbsTol', 1e-6);

        % Total root-mean-square pressure level and corresponding SPL
        prmsNearField(i) = sqrt(2) / (8 * pi^2) * sqrt(intA^2 + intB^2);
        SPLNearField(i) = 20 * log10(prmsNearField(i) / pref);

    end
end
```

```matlab
function [prmsNearFieldSphere, SPLNearFieldSphere, x, y, z] = prmsNearFieldSphere↩
    (m, B, D, M, T, Q, rpm, c0, azimuth, elevation)
% Created for MATLAB 2020a or later
```

```matlab
    syms theta % Variable of integration
    omega = 2 * pi * rpm / 60; % Angular speed
    k = m * B * omega / c0; % Wave number
    beta = sqrt(1 - M^2);
    R_e = 0.8 * (D / 2); % Effective radius

    % Loading coordinates
    x_l = @(theta) 0;
    y_l = @(theta) R_e * cos(theta);
    z_l = @(theta) R_e * sin(theta);

    % Predefined to reduce runtime
    prmsNearFieldSphere = zeros(length(azimuth));
    SPLNearFieldSphere = zeros(length(azimuth));
    pref = 2e-5; % Reference pressure 20*10^(-6) Pa

    % Field points created to decrease runtime
    x = zeros(length(azimuth));
    y = zeros(length(azimuth));
    z = zeros(length(azimuth));

    for i = 1 : length(azimuth)
        for j = 1 : length(azimuth)

            % Field points, default radius 2D
            x(i,j) = 2 * D * cos(elevation(j));
            y(i,j) = 2 * D * cos(azimuth(i)) * sin(elevation(j));
            z(i,j) = 2 * D * sin(azimuth(i)) * sin(elevation(j));

            S = @(theta) sqrt((x(i,j) - x_l(theta)).^2 + beta^2 * ((y(i,j) - y_l(←
                theta)).^2 + (z(i,j) - z_l(theta)).^2));
            sigma = @(theta) (M * (x(i,j) - x_l(theta)) + S(theta)) / beta^2;

            % Functions to integrate
            funA = @(theta) (T .* x(i,j) ./ S(theta).^2 .* cos(m * B .* theta + k←
                 .* sigma(theta))...
                + (T * k / beta^2 * (M + x(i,j) ./ S(theta)) - Q * m * B / R_e^2)←
                    ...
                .* sin(m * B .* theta + k .* sigma(theta))) ./ S(theta);
            funB = @(theta) (-T .* x(i,j) ./ S(theta).^2 .* sin(m * B .* theta + ←
                k .* sigma(theta))...
                + (T * k / beta^2 * (M + x(i,j) ./ S(theta)) - Q * m * B / R_e^2)←
                    ...
                .* cos(m * B .* theta + k .* sigma(theta))) ./ S(theta);

            % Integrals
            intA = integral(funA, 0, 2 * pi, 'RelTol', 1e-6, 'AbsTol', 1e-6);
            intB = integral(funB, 0, 2 * pi, 'RelTol', 1e-6, 'AbsTol', 1e-6);

            % Total root-mean-square pressure level and corresponding SPL
            prmsNearFieldSphere(i,j) = sqrt(2) / (8 * pi^2) * sqrt(intA^2 + intB←
                ^2);
            SPLNearFieldSphere(i,j) = 20 * log10(prmsNearFieldSphere(i,j) / pref)←
                ;

        end
    end
end
```

```matlab
function [prmsFarField, SPLFarField] = prmsFarField(m, B, D, M, c0, rpm, T, Q, x,←
     y)
% Created for MATLAB 2020a or later

    omega = 2 * pi * rpm / 60; % Angular speed
    k = m * B * omega / c0; % Wave number
    beta = sqrt(1 - M^2);
    R_e = 0.8 * (D / 2); % Effective radius
    z = 100 * D; % Altitude of propeller, default 100D
```

```matlab
    omega1 = B * omega;
    nu = m * B; % Order of Bessel function

    % Predefined to reduce runtime
    prmsFarField = zeros(size(x, 1), size(x, 2));
    SPLFarField = zeros(size(x, 1), size(x, 2));
    pref = 2e-5; % Reference pressure 20*10^(-6) Pa

    % Input matrices x and y should be equal in size, each matrix element an ←
        observer
    for i = 1 : size(x, 1)

        for j = 1 : size(x, 2)

            S0 = sqrt(x(i,j)^2 + y(i,j)^2 + beta^2 * z^2);

            Z = k * z * R_e / S0; % Argument for Bessel function

            % Total root-mean-square pressure level and corresponding SPL
            prmsFarField(i,j) = m * omega1 / (sqrt(8) * pi * c0 * S0)...
                    .* abs(T * (M + x(i,j) / S0) / beta^2 - Q * B * c0 / (omega1 ←
                        * R_e^2))...
                    .* besselj(nu, Z);
            SPLFarField(i,j) = 20 * log10(prmsFarField(i,j) / pref);

        end
    end
end
```

B.2.2 Multiple Propellers

```matlab
clear
close all
clc
tic

format long;

set(0,'DefaultLineLineWidth',1.1)
set(0,'DefaultaxesLineWidth',1)
set(0,'DefaultaxesFontSize',16)
set(0,'defaultAxesTickLabelInterpreter','latex')
set(0,'defaultLegendInterpreter','latex')

%++++++++++++++++++++++++++++++++++++++++++++++++++++++++++++++++++++++++++%
%++++++++++++++++++++++++++++++++++++++++++++++++++++++++++++++++++++++++++%
%++++++++++++++++++++++++++++++++++++++++++++++++++++++++++++++++++++++++++%
%%
PropNum = 3; %number of propellers
ThrustCoeff = [0.136991488, 0.091327658 0.068495744,0.045663829];
PropEf = [88.018555,90.532078,90.860559,89.669629];
%%
if PropNum == 2
ThrustCoef = ThrustCoeff(1);
PropEff = PropEf(1)/100;
elseif PropNum == 3
ThrustCoef = ThrustCoeff(2);
PropEff = PropEf(2)/100;
elseif PropNum == 4
ThrustCoef = ThrustCoeff(3);
PropEff = PropEf(3)/100;
elseif PropNum == 6
ThrustCoef = ThrustCoeff(4);
PropEff = PropEf(4)/100;
end
%============================
```

```matlab
GeoAndOperParas = importdata('PropGeoOperParas.dat');
D = GeoAndOperParas(1); % diameter
BNum = GeoAndOperParas(2);  %  blade number
RPM = GeoAndOperParas(3);   % rotational speed
angularspeed = RPM*2*pi/60; % angular speed (rad/s)
CruiseMach = GeoAndOperParas(4);    % cruise Mach number

%============================

EnviroParas = importdata('EnviroParas.dat');
CruiseH = EnviroParas(1);   % cruise altitude
CruiseT = EnviroParas(2);   % cruise temperature
CruiseP = EnviroParas(3);   % cruise pressure
CruiseRho = CruiseP/287/CruiseT;    % cruise density
CruiseSoundSpeed = sqrt(1.4*287*CruiseT);   % cruise sound speed
pref = 2e-5; % reference acoustic pressure (Pa);

%++++++++++++++++++++++++++++++++++++++++++++++++++++++++++++++++++++++++++%
%++++++++++++++++++++++++++++++++++++++++++++++++++++++++++++++++++++++++++%

jk = 0; % counting

XNum1 = 101; %number of observers in x
ZNum1 = 1; %number of observers in z

xfar1 = linspace(-10*D,10*D,XNum1);
zfar1 = linspace(-2*D,2*D,ZNum1);

for j = 1 : XNum1

    for k = 1 : ZNum1

        jk = jk + 1;

        x1(jk) = xfar1(j);
        y1(jk) = -4*D;
        z1(jk) = 0; % zfar(k);

    end

end

ONum1 = jk; % number of observers

% farfield observers

kj = 0;
XNum2 = 101;
ZNum2 = 1;

xfar2 = linspace(-100*D,100*D,XNum2);
zfar2 = linspace(-10*D,10*D,ZNum2);

for j = 1 : XNum2

    for k = 1 : ZNum2

        kj = kj + 1;

        x2(kj) = xfar2(j);
        y2(kj) = -100*D;
        z2(kj) = 0; % zfar(k);

    end

end

ONum2 = kj; % % number of farfield observers
```

```matlab
figure(1) % plots a circle at each observer
scatter3(x1,y1,z1,'k'); %near field

figure(2)
scatter3(x2,y2,z2,'k'); % far field

%++++++++++++++++++++++++++++++++++++++++++++++++++++++++++++++++++++++++%
%++++++++++++++++++++++++++++++++++++++++++++++++++++++++++++++++++++++++%

Thrust = ThrustCoef*CruiseRho*(RPM/60)^2*D^4;    % cruise thrust
Torque = Thrust*CruiseMach*CruiseSoundSpeed/PropEff/angularspeed;  %cruise torque
Re = 0.8*D/2;    % effective radius
HNum = 1;    % harmonic number
AZNum = 3601;    % azimuthal number for blade
TNum = 128;    %time number
Beta = sqrt(1-CruiseMach^2); %same beta as before

if PropNum == 6 % Distribution 4
PropXCoord = [0*D;0*D;0*D;0*D;0*D;0*D]; %% propeller coordinates
PropZCoord = [-2*D;2*D;-4*D;4*D;-3*D;3*D];
elseif PropNum == 4 % Distribution 3
PropXCoord = [0*D;0*D;0*D;0*D];
PropZCoord = [-3*D;-2*D;2*D;3*D];
elseif PropNum == 3 % Distribution 2
PropXCoord = [0*D;-5*D;0*D];
PropZCoord = [-2*D;0*D;2*D];
elseif PropNum == 2 % Distribution 1
PropXCoord = [0*D;0*D];
PropZCoord = [-2*D;2*D];
end

%%

m = 1;

Time = linspace(0,2*pi/(m*BNum*angularspeed),TNum); %time vector
kc = m*BNum*angularspeed/CruiseSoundSpeed;

PT1 = zeros(TNum,ONum1,PropNum);
PQ1 = zeros(TNum,ONum1,PropNum);
TP1 = zeros(TNum,ONum1,PropNum);
TPProp1 = zeros(TNum,ONum1);
TPrms1 = zeros(1,ONum1);
SPL1 = zeros(1,ONum1);

for j = 1 : ONum1

    for t = 1 : TNum

        for k = 1 : PropNum

            % observers
            ox = x1(j);
            oy = y1(j);
            oz = z1(j);

            % sources positions over time
            stheta = linspace(0,2*pi,AZNum);
            sx = 0+PropXCoord(k);
            sy = Re*cos(stheta);
            sz = PropZCoord(k)+Re*sin(stheta);

            %
            S = sqrt((ox-sx).^2+Beta^2*((oy-sy).^2+(oz-sz).^2));
            Sigma = (CruiseMach*(ox-sx)+S)/Beta^2;
            %
            AS = Thrust*(1i*kc*CruiseMach/Beta^2+1i*kc*ox./(Beta^2*S)+ox./S.^2)↩
                ...
                .*exp(-1i*(m*BNum*stheta+kc*Sigma))./S;
            BS = Torque*1i*m*BNum/Re^2 ...
```

```matlab
                    .*exp(-1i*(m*BNum*stheta+kc*Sigma))./S;

            % integration using the Trapezoidal Rule
            A = (2*sum(AS)-AS(1)-AS(AZNum))*(2*pi/AZNum)/2;
            B = (2*sum(BS)-BS(1)-BS(AZNum))*(2*pi/AZNum)/2;

            PT1(t,j,k) = exp(1i*m*BNum*angularspeed*Time(t))*A/4/pi^2; % equation↵
                [24]
            PQ1(t,j,k) = -exp(1i*m*BNum*angularspeed*Time(t))*B/4/pi^2; % ↵
                equation [25]
            TP1(t,j,k) = PT1(t,j,k) + PQ1(t,j,k);

        end

        TPProp1(t,j) = sum(TP1(t,j,:)); % calculates total pressure from all ↵
            propellers.
    end

    TPrms1(j) = rms(TPProp1(t,j))/sqrt(2); %calculates rms value
    SPL1(j) = 20*log10(TPrms1(j)/pref); % converts the pressure to decibel

end

% farfield

PT2 = zeros(TNum,ONum2,PropNum);
PQ2 = zeros(TNum,ONum2,PropNum);
TP2 = zeros(TNum,ONum2,PropNum);
TPProp2 = zeros(TNum,ONum2);
TPrms2 = zeros(1,ONum2);
SPL2 = zeros(1,ONum2);

for j = 1 : ONum2

    for t = 1 : TNum

        for k = 1 : PropNum

            % observers
            ox = x2(j);
            oy = y2(j);
            oz = z2(j);

            % sources positions over time
            stheta = linspace(0,2*pi,AZNum);
            sx = 0+PropXCoord(k);
            sy = Re*cos(stheta);
            sz = PropZCoord(k)+Re*sin(stheta);

            %
            S0 = sqrt(ox^2+Beta^2*oy^2);

            %
            PT2(t,j,k) = exp(1i*m*BNum*angularspeed*Time(t))*Thrust/(2*pi*S0)...
                    *(1i)^(m*BNum)*exp(-1i*kc/Beta^2*(S0+CruiseMach*ox))...
                    *1i*kc/Beta^2*(CruiseMach+ox/S0)...
                    *besselj(m*BNum,kc*Re*oy/S0);
            PQ2(t,j,k) = -exp(1i*m*BNum*angularspeed*Time(t))*Torque/(2*pi*S0*Re↵
                ^2)...
                    *(1i)^(m*BNum+1)*m*BNum*exp(-1i*kc/Beta^2*(S0+CruiseMach*↵
                        ox))...
                    *besselj(m*BNum,kc*Re*oy/S0);
            TP2(t,j,k) = PT2(t,j,k) + PQ2(t,j,k);

        end

        TPProp2(t,j) = sum(TP2(t,j,:)); % sum of both propellers pressure

    end
```

```matlab
    TPrms2(j) = rms(TPProp2(t,j))/sqrt(2); % calculate rms
    SPL2(j) = 20*log10(TPrms2(j)/pref); % converts to decibel

end

%% Post-processing
a(4,:) = SPL1;
b(4,:) = SPL2;
SPLAZ1 = cell(1,HNum); %predefine cell matrix with 1xHarmonic number dimensions
SPLAZ2 = cell(1,HNum);

for m = 1 : HNum
    % converts decibel vectors to matrix
    SPLAZ1{m} = reshape(SPL1(m,:),[length(zfar1),length(xfar1)]);
    SPLAZ2{m} = reshape(SPL2(m,:),[length(zfar2),length(xfar2)]);

end

figure(3)
grid on
plot(x1,SPLAZ1{1}(1,:),'r-o'); % plots the decibel at each observer with a red ←
    circle in the near field
xlabel('x, [m]');
ylabel('SPL, dB');

set(gca,'FontName','Times New Roman','FontSize',16);
box off
%
figure(4)
grid on
plot(x2,SPLAZ2{1}(1,:),'r-o'); % plots the decibel at each observer with a red ←
    circle in the far field
xlabel('x, [m]');
ylabel('SPL, dB');

set(gca,'FontName','Times New Roman','FontSize',16);
box off
%%
% Outputd data
%
fid = fopen('NearfieldSPL_2.dat','w'); % opens the .dat file, 'w' causes all ←
    existing data to be overwritten
fprintf(fid,'%d %s\n',ONum1,'observer number'); % adds data to .dat file
fprintf(fid,'%e %s\n',BNum*angularspeed/2/pi,':blade passing frequency'); % adds ←
    data to .dat file
for j = 1 : ONum1

    fprintf(fid,'%e %e %e %e\n',x1(j),y1(j),z1(j),SPL1(j)); %adds data from every←
        observer to .dat

end
fclose(fid); %closes the .dat file

%
fid = fopen('FarfieldSPL_2.dat','w');
fprintf(fid,'%d %s\n',ONum2,'observer number');
fprintf(fid,'%e %s\n',BNum*angularspeed/2/pi,':blade passing frequency');
for j = 1 : ONum2

    fprintf(fid,'%e %e %e %e\n',x2(j),y2(j),z2(j),SPL2(j));

end
fclose(fid);
%%
toc
```